Search for H → WW* Production at CDF Using 9.7 fb^{-1} of Data

Text for the public web page – CDF note 10760

The CDF Collaboration
URL http://www-cdf.fnal.gov
(Dated: March 1, 2012)

We report a search for Standard Model (SM) Higgs boson to WW^* production in the two charged lepton (e, μ) and two neutrino final state in $p\overline{p}$ collisions at $\sqrt{s} = 1.96$ TeV. The data were collected with the CDF II detector at the Tevatron collider at Fermilab and correspond to an integrated luminosity of approximately 9.7 fb^{-1}. In order to maximize sensitivity, three neural networks are separately trained to distinguish signal from background processes in final states with either zero, one, or two or more jets. For 0-jet events, likelihood ratios based on Matrix Element calculations are used as additional inputs to the neural network to further strengthen its discriminating power. In order to take advantage of the maximum potential signal acceptance, we also consider associated production with a W or Z boson and Higgs boson production via vector boson fusion. Additional signal acceptance is gained by including events with low dilepton invariant mass as a separate search region. We also search for associated Higgs production in events with same-sign dileptons and trileptons in the final state. In the opposite-sign event sample we observe (summing over all jet multiplicities) a total of 4167 candidate events compared against an expectation of 4040 ± 340 background events and 63.0 ± 9.1 signal events for a SM Higgs boson with a mass of 165 GeV/c^2. In the opposite-sign low dilepton invariant mass sample we observe 319 candidate events compared against an expectation of 291 ± 19 background events and 4.41 ± 0.68 signal events for a SM Higgs boson with a mass of 165 GeV/c^2. In the same-sign event sample we additionally observe 87 candidate events compared with an expectation of 85 ± 18 background events and 3.08 ± 0.41 signal events for a SM Higgs boson with a mass of 165 GeV/c^2. In the trilepton event sample we observe 84 candidate events compared with an expectation of 79.2 ± 9.5 background events and 2.49 ± 0.34 signal events for a SM Higgs boson with a mass of 165 GeV/c^2. Based on these samples, we determine an observed 95% C.L. upper production limit of 0.40 times the SM prediction at NNLL for a Higgs mass of 165 GeV/c^2 to be compared with the value for the median of the expected limit (0.69). Results for eighteen other Higgs mass hypotheses ranging from 110 GeV/c^2 to 200 GeV/c^2 are also presented. We exclude at the 95% C.L. a SM Higgs boson in the mass range between 148 and 175 GeV/c^2. We also present a separate search for a SM Higgs boson considering only the $gg \to H \to W^+W^-$ production process using a 8.2 fb^{-1} data sample. In this case we circumvent theoretical cross section uncertainties and obtain 95% C.L. upper limits on the production cross section times branching ratio for this process. We extract these limits for twenty-nine different Higgs mass hypotheses in the range between 110 GeV/c^2 and 300 GeV/c^2. Using these limits we place constraints on a potential Higgs mass in the scenario of a fourth sequential generation of fermions with large masses, which would lead to significantly enhanced $gg \to H$ production. For this scenario we exclude at the 95% C.L. a SM-like Higgs boson in the mass range between 121 and 207 GeV/c^2. Additionally, a fermiophobic search is carried out. To perform this search, gluon fusion SM Higgs production is removed and the $H \to \gamma\gamma$ final state is added. For eleven different Higgs

masses, we extract 95% C.L. upper limits on the production cross section times branching ratio for this process in the range between 100 GeV/c^2 and 200 GeV/c^2. For this scenario we exclude at the 95% C.L. a fermiophobic Higgs boson in the mass range between 100 and 115 GeV/c^2.

PACS numbers:

I. INTRODUCTION

The Higgs boson is introduced into the Standard Model (SM) to explain electroweak symmetry breaking and the origins of particle mass. Current precision electroweak measurements constrain the mass of a SM Higgs boson to be less than 158 GeV/c^2 (one-sided 95% C.L. upper limit) or 185 GeV/c^2 when including the LEP-2 direct search lower bound limit of 114 GeV/c^2 at 95% C.L. [1]. For this analysis we focus on the Higgs decaying to WW^*, which is the dominant decay channel for $m_H > 135$ GeV/c^2 [2]. The small cross section of the dominant gluon fusion production mechanism ($\sigma_{NNLL}(gg \to H) = 0.439$ pb for m_H =160 GeV/c^2 [3] [4]) makes observation of the signal difficult within the hadron collider environment.

In this note, we present a search for $gg \to H \to WW^* \to \ell^+\ell^-\nu\bar{\nu}$, where $\ell^\pm = e$, μ or τ in the final states e^+e^-, $e^\pm\mu^\mp$ and $\mu^+\mu^-$. We extend our search to include Higgs bosons produced in vector boson fusion and in associated production with either a Z boson ($ZH \to ZWW^*$) or a W boson ($WH \to WWW^*$). We also search for associated Higgs production in events with two like sign leptons, with final states $e^\pm e^\pm$, $e^\pm\mu^\pm$ and $\mu^\pm\mu^\pm$. We additionally search for associated Higgs production in events with three leptons (e or μ) where one has the opposite charge of the other two. We use approximately 9.7 fb^{-1} of integrated luminosity collected by the CDF II detector at the Fermilab Tevatron with $p\bar{p}$ collisions at $\sqrt{s} = 1.96$ TeV.

The analysis strategy is to use a common event selection, described in Sec. IV, for 19 different Higgs mass hypotheses between 110 GeV/c^2 and 200 GeV/c^2. For each Higgs mass point, a NeuroBayes® [5] neural network is trained to distinguish signal from background on a weighted combination of known signal and background events. To maximize sensitivity, different choices of kinematic inputs to the neural network are made for each final state considered separately: opposite-sign events with zero jets, opposite-sign events with one jet, opposite-sign events with two or more jets, opposite-sign events with low dilepton invariant mass ($M_{\ell\ell}$) and zero or one jet, same-sign events with one or more jets, trilepton events with no same-flavor opposite-sign dilepton pair in the Z-mass peak, trilepton events with a same-flavor opposite-sign dilepton pair in the Z-mass peak and 1 jet, and trilepton events with a same-flavor opposite-sign dilepton pair in the Z-mass peak and two or more jets. In the opposite-sign 0-jet analysis, additional inputs to the neural networks are based on Matrix Element calculations for the event probability densities for the different background and signal processes using leading order matrix elements from the MCFM [6] package. In opposite-sign two or more jets events, an additional selection criteria is made to veto events with a jet that has been tagged as coming from a b quark in order to suppress the dominant $t\bar{t}$ background. The criteria to include opposite-sign events with low $M_{\ell\ell}$ is described in Sec. IV B. The criteria used to select same-sign events is modified as described in Sec. IV C to optimize the ratio of signal to background in this channel. The criteria used to select trilepton events is described in Sec. IV D. Templates from the neural network output in each of the three jet multiplicity, low $M_{\ell\ell}$, same-sign, and the three trilepton channels corresponding to the expected background and signal contributions are then compared to the neural network data templates. A likelihood method is used to calculate the 95% C.L. limits on Higgs production relative to the SM expectation based on predicted and observed neural network output templates.

We also test a natural extension to the SM using a 8.2 fb^{-1} data sample in which there exists a fourth generation of fermions with masses much larger than those of the three known generations. In this scenario, precision electroweak measurements allow for a heavy Higgs boson up to $m_H \sim 300$ GeV at the 68% C.L. A consequence of the extra fermions is a factor of three enhancement in the ggH coupling, which leads to a substantial increase in the $gg \to H$ production cross section. To place constraints on a SM-like Higgs in the context of a fourth generation model, we reproduce our SM Higgs search focusing solely on Higgs production through the gluon fusion process. We restrict the search to our opposite-sign zero, one, and two or more jet channels, which contain most of our signal acceptance to gluon fusion produced Higgs events. We do not modify the event selection for these channels but do retrain the corresponding neural networks using pure, simulated samples of gluon produced Higgs events in contrast to the mixed production samples used in SM searches. Since we consider a single production process, we are able to avoid theoretical uncertainties and obtain direct upper limits on the gluon fusion production cross section. The cross section limits are extracted for twenty-nine different Higgs mass hypotheses in the range from 110 to 300 GeV/c^2. Finally, based on theoretical fourth generation model cross section predictions [7], we obtain from these limits an excluded mass range at 95% C.L. for a SM-like Higgs boson within the framework of the fourth generation model.

Additionally, a fermiophobic search is carried out. In the SM, the $H \to \gamma\gamma$ branching fraction is quite small. For a fermiophobic Higgs however, the decay of the Higgs to fermions is suppressed, thereby enhancing $H \to \gamma\gamma$. For this search, gluon Higgs production is removed and the Higgs final state of $\gamma\gamma$ is added. Production of Higgs bosons in association with a W or Z boson and vector boson fusion are kept from the $H \to WW$ analysis. Specifics of the $H \to \gamma\gamma$ search can be found in [8]. For eleven different Higgs masses, we extract 95% C.L. upper limits on the production cross section times branching ratio for this process in the range between 100 GeV/c^2 and 150 GeV/c^2.

II. DETECTOR DESCRIPTION

The components of the CDF II detector relevant to this analysis are described briefly here; a more complete description can be found elsewhere [9]. The detector geometry is described by the azimuthal angle ϕ and the pseudo-rapidity $\eta \equiv -\ln(\tan\theta/2)$, where θ is the polar angle of a particle with respect to the proton beam axis (positive z-axis). The pseudo-rapidity of a particle originating from the center of the detector is referred to as $\eta_{\rm det}$.

The trajectories of charged particles are reconstructed using silicon micro-strip detectors [10][11] and a 96-layer open-cell drift chamber (COT) [12] embedded in a 1.4 T solenoidal magnetic field. For $|\eta_{\rm det}| \leq 1$, a particle traverses all 96 layers of the COT; this decreases to zero at $|\eta_{\rm det}| \approx 2$. The silicon system provides coverage with 6 (7) layers with radii between 2.4 cm and 28 cm for $|\eta_{\rm det}| < 1.0$ ($1.0 < |\eta_{\rm det}| < 2.0$). Outside of the solenoid are electromagnetic (EM) and hadronic (HAD) sampling calorimeters segmented in a projective tower geometry. The first hadronic interaction length (λ) of the calorimeter, corresponding to 19-21 radiation lengths (X_0), uses lead absorber for measuring the electromagnetic component of showers, while the section extending to 4.5-7 λ uses iron to contain the hadronic component. The calorimeters are divided in a central ($|\eta_{\rm det}| < 1$) and forward ($1.1 < |\eta_{\rm det}| < 3.64$) region. Shower maximum detectors (SMX) embedded in the electromagnetic calorimeters at approximately $6X_0$ help in the position measurement and background suppression for electrons. Outside of the central calorimeters are scintillators and drift chambers for identifying muons as minimum ionizing particles. We use three complementary track pattern recognition algorithms which are distinguished by their starting point in COT, silicon, or projection from calorimeter energy cluster to interaction region.

III. LEPTON IDENTIFICATION

In order to maximize signal acceptance and suppress backgrounds from jets and photons misidentified as leptons, we use two (eight) categories of electrons (muons). Two additional categories, based on central tracks that are not fiducial to calorimeters or muon detectors, is used as either an electron or muon in forming $H \to WW^*$ candidates. The resulting categories exploit essentially all the tracks and electromagnetic calorimeter clusters available.

All leptons are required to be isolated such that the sum of the E_T for the calorimeter towers in a cone of $\Delta R = \sqrt{(\Delta\eta)^2 + (\Delta\phi)^2} < 0.4$ around the lepton is less than 10% of the electron E_T or muon p_T. If an additional good muon or electron candidate is found within the $\Delta R < 0.4$ cone, the towers the additional lepton passed through are subtracted from the E_T sum. The transverse energy E_T of a shower or calorimeter tower is $E \sin\theta$, where E is the associated energy. Similarly, p_T is the component of track momentum transverse to the beam line.

Electron candidates are required to have a ratio of HAD energy to EM energy consistent with originating from an electromagnetic shower and are further divided into central and forward categories. The central electron category requires a well-measured COT track satisfying $p_T > 10$ GeV/c that is fiducial to the central SMX and matched to a central EM energy cluster. Central electron candidates are then selected using a likelihood method to combine electron identification variables into one discriminant. A forward electron is required to be fiducial to the forward SMX detector and have energy deposition in both the calorimeter towers and SMX detector consistent with an electron shower shape. For each foward candidate, we also require a matching calorimeter seeded track that is consistent with a standalone reconstructed track formed using hits in the silicon detector to reduce background from photons. If a forward electron fails this cut based category, it has a chance to pass using a likelihood based discriminant.

Muons are identified by either a charged track matched to a reconstructed track segment ("stub") in muon chambers or as a stubless minimum ionizing particle fiducial to calorimeters. In addition, stubless muons are required to have at least 0.1 GeV in total calorimeter energy. For $|\eta_{\rm det}| < 1.2$, strict requirements on the number of COT hits and the χ^2 of the track fit are placed on the muon tracks in order to suppress kaon decay-in-flight backgrounds. The category of stubless muons with $|\eta_{\rm det}| > 1.2$ requires that at least 60% of the COT layers crossed by the track have hits. In order to suppress background from cosmic rays, the track's point of closest approach to the beamline must be consistent with originating from the beam.

The final category of leptons are constructed from tracks which are not fiducial to the SMX detectors nor identified as stubbed muons. The requirements for the tracks are the same as stubless muons with $|\eta_{\rm det}| < 1.2$, but without any of the calorimeter requirements. Due to the lack of calorimeter information, electron and muons cannot be reliably differentiated in this region, and this category is therefore treated as having either flavor in the Higgs candidate selection. If an electron or non-fiducial track candidate is consistent with being due to a photon conversion as indicated by the presence of an additional nearby track, the candidate is vetoed.

To identify the presence of a Higgs boson decaying to two neutrinos, we use the missing transverse energy $\not\!\!E_T = |\sum_i E_{T,i}\ \hat{n}_{T,i}|$, where the $\hat{n}_{T,i}$ is the transverse component of the unit vector pointing from the interaction point to calorimeter tower i. The $\not\!\!E_T$ is corrected for muons which do not deposit all of their energy in the calorimeter and tracks which point to uninstrumented regions of the calorimeter.

TABLE I: Expected and observed yields for background and signal for opposite-sign dilepton events with 0 jets in the final state.

CDF Run II Preliminary $\int \mathcal{L} = 9.7$ fb^{-1}		
$M_H = 165$ GeV/c^2		
$t\bar{t}$	3.9 ±	1.2
DY	430 ±	120
WW	969 ±	97
WZ	44.6 ±	6.8
ZZ	63.5 ±	9.0
W+jets	581 ±	74
$W\gamma$	249 ±	31
Total Background	2340 ±	210
$gg \to H$	28.9 ±	8.6
WH	0.72 ±	0.12
ZH	0.70 ±	0.10
VBF	0.253 ±	0.052
Total Signal	30.6 ±	8.7
Data	2538	

A1lSB-0J

The Higgs candidate events are required to pass one of five online trigger selections implemented in three successively more stringent levels. The final central electron requirement is an EM energy cluster with $E_T > 18$ GeV matched to a track with $p_T > 8$ GeV/c. Muon triggers are based on information from muon chambers matched to a track with $p_T > 18$ GeV/c. The trigger for forward electrons requires an $E_T > 20$ GeV EM energy cluster and an online measurement of the $\not\!\!E_T > 15$ GeV.

IV. EVENT SELECTION

A. Opposite-sign Base Selection

The $\ell\ell\nu\overline{\nu}$ candidates are selected from two opposite-sign leptons. At least one lepton is required to satisfy the trigger and have $E_T > 20$ GeV ($p_T > 20$ GeV/c) for electrons (muons). We loosen this requirement to > 10 GeV (GeV/c) for the second lepton to increase Higgs kinematic acceptance. The z-positions of the leptons in a candidate at the point of closest approach to the beam-line are required to be within 4 cm of each other.

There are several sources of background: Drell-Yan where the measured large $\not\!\!E_T$ is due to resolution tails, $WZ \to \ell\ell\ell\nu$ where one lepton is lost, $WW \to \ell\ell\nu\overline{\nu}$, $t\bar{t} \to b\bar{b}\ell\ell\nu\overline{\nu}$, and $W\gamma/W$+jets where a photon or jet is misidentified as a lepton. Because of the significant backgrounds from $W\gamma$ and W+jets, we apply an additional isolation requirement on the leptons that the sum of the track p_T in a cone for $\Delta R < 0.4$ around each lepton is less than 10% of the electron E_T or muon p_T. This requirement is dropped for electrons selected using the likelihood method.

To suppress the Drell-Yan background, we require $\not\!\!E_{T\mathrm{spec}} > 25$ GeV (reduced to $\not\!\!E_{T\mathrm{spec}} > 15$ GeV for electron-muon events for which the Drell-Yan background is inherently smaller), where $\not\!\!E_{T\mathrm{spec}}$ is defined to be:

$$\not\!\!E_{T\mathrm{spec}} \equiv \begin{cases} \not\!\!E_T & \text{if } \Delta\phi(\not\!\!E_T, \text{nearest lepton or jet}) > \frac{\pi}{2} \\ \not\!\!E_T \sin(\Delta\phi(\not\!\!E_T, \text{nearest lepton or jet})) & \text{if } \Delta\phi(\not\!\!E_T, \text{nearest lepton or jet}) < \frac{\pi}{2} \end{cases}$$

This definition is a requirement that the transverse component of $\vec{\not\!\!E}_T$ relative to each lepton or jet in an event lies above a default threshold. This ensures that events in which the $\vec{\not\!\!E}_T$ is generated primarily from the mismeasurement of a single object will not enter the sample. We further require the candidates to have $M_{\ell\ell} > 16$ GeV/c^2 to suppress $W\gamma$ contributions, and exactly 2 leptons to suppress WZ contributions with a third lepton.

We consider individually final states with no jets in the event, one jet, or two or more jets where a jet is required to have $E_T > 15$ GeV and $|\eta| < 2.5$. This allows us to tune our multivariate discriminants on the different mixes of signal and background contributions within each jet multiplicity bin. In order to suppress the dominant $t\bar{t}$ background in the two or more jets bin, all events containing jets with a tight, secondary vertex b-tag are rejected.

The expected and observed yields after base selection cuts have been applied are shown for the three jet multiplicity channels in Tables I-III.

TABLE II: Expected and observed yields for background and signal for opposite-sign dilepton events with 1 jet in the final state.

CDF Run II Preliminary $\int \mathcal{L} = 9.7$ fb^{-1}		
$M_H = 165$ GeV/c^2		
$t\bar{t}$	100 ±	19
DY	421 ±	97
WW	261 ±	32
WZ	42.4 ±	5.9
ZZ	17.2 ±	2.5
W+jets	217 ±	30
$W\gamma$	41.5 ±	6.4
Total Background	1100 ±	130
$gg \to H$	14.4 ±	6.1
WH	1.93 ±	0.31
ZH	0.74 ±	0.12
VBF	1.34 ±	0.23
Total Signal	18.4 ±	6.2
Data	1033	

AllSB-1J

TABLE III: Expected and observed yields for background and signal for opposite-sign dilepton events with 2 or more jets in the final state.

CDF Run II Preliminary $\int \mathcal{L} = 9.7$ fb^{-1}		
$M_H = 165$ GeV/c^2		
$t\bar{t}$	287 ±	42
DY	150 ±	64
WW	53 ±	12
WZ	11.7 ±	2.2
ZZ	5.3 ±	1.0
W+jets	80 ±	15
$W\gamma$	8.3 ±	2.1
Total Background	596 ±	96
$gg \to H$	5.0 ±	2.5
WH	4.35 ±	0.61
ZH	2.16 ±	0.29
VBF	2.51 ±	0.41
Total Signal	14.0 ±	2.9
Data	596	

AllSB-2JOS

B. Low $M_{\ell\ell}$ Base Selection

To increase signal acceptance, we consider separately events which fail only the $M_{\ell\ell} > 16$ GeV/c^2 requirement of the opposite-sign signal region selection. Events containing leptons with energies in excess of 400 GeV are rejected, and only events with zero or one jets are considered. Heavy flavor contributions ($J/\psi, \Upsilon$) are effectively removed by the $\not\!\!E_{T\mathrm{spec}}$ requirements and an additional cut on $\not\!\!E_T$ significance based on the sum of lepton and jet energies ($\not\!\!E_T/\sqrt{\Sigma E_{\mathrm{T}}(\mathrm{leptons,jets})}$) $\not\!\!E_T/\sqrt{\Sigma E_{\mathrm{T}}(\mathrm{leptons,jets})} > 4$ if $M_{\ell\ell} < 6$ GeV/c^2 or $8.5 < M_{\ell\ell} < 10.5$ GeV/c^2. Boson Radiation (BosRad) processes with radiation of a Z boson from a final state quark and having an off-shell mass, M_{Z0} in the range $6 < M_{Z0} < 16$ GeV/c^2 have been computed using MadGraph4 [13]. The primary background in this selection region is $W\gamma$ events, where the photon is misidentified as a lepton.

Events with this selection but containing two same-sign leptons form a control sample to test the $W\gamma$ background model. This control sample is composed primarily of $W\gamma$ events, which contribute about 87%, and is used to estimate a correction factor for the $W\gamma$ Monte Carlo and systematic uncertainties on the modeling of $W\gamma$ events.

Events with this selection but having $15 < \not\!\!E_{T\mathrm{spec}} < 25$ GeV form a control region to test for the presence of Heavy flavor resonances and Boson Radiation. This control sample is used to test for evidence of heavy flavor resonances remains after the $\not\!\!E_T/\sqrt{\Sigma E_{\mathrm{T}}(\mathrm{leptons,jets})}$ and $M_{\ell\ell}$ cuts and is used to estimate a corection factor for the Boson Radation contribution and systematic uncertainties in the modeling of Boson Radiation.

TABLE IV: Expected and observed yields for background and signal for events with $M_{\ell\ell} < 16$ GeV/c^2 and either 0 or 1 jets in the final state.

CDF Run II Preliminary $\int \mathcal{L} = 9.7$ fb^{-1}	
$M_H = 165$ GeV/c^2	
$t\bar{t}$	1.82 ± 0.35
DY	23.9 ± 4.9
WW	37.5 ± 3.6
WZ	0.96 ± 0.13
ZZ	0.292 ± 0.041
W+jets	56.3 ± 7.8
$W\gamma$	171 ± 14
Total Background	291 ± 19
$gg \to H$	4.02 ± 0.66
WH	0.140 ± 0.023
ZH	0.109 ± 0.016
VBF	0.146 ± 0.026
Total Signal	4.41 ± 0.68
Data	319

A11SB-lowM11

The expected and observed yields after these selection cuts have been applied are shown in Table IV.

C. Same-sign Base Selection

To increase sensitivity, we also search for Higgs signal in like sign, or same-sign (SS), dileptons. These occur naturally in $VH \to VWW$ production, when the vector boson (Z or W) and one of the W bosons from the Higgs decay leptonically. The majority of background events in this search originate from either a charge misidentification of a real lepton or the reconstruction of a fake lepton from a photon or jet.

In addition to selecting events with two like sign leptons, modifications are made to the base selection criteria used for opposite-sign events to further reduce these backgrounds. In particular, we do not accept events containing forward electrons, which have a high charge mismeasurement rate. In addition, central electron candidates are required to pass standard tight selection cuts as opposed to being selected using the looser likelihood selection criteria. To further reduce the number of photons or jets misidentified as leptons, the $p_{\rm T}$ requirement for the second lepton is increased from 10 GeV/c to 20 GeV/c. Since the decay of the third boson most often results in the production of additional jets, we also require one or more jets in the final state. Events with two same-sign electrons are prone to a significant background contribution from trident events, which are not modeled well kinematically by Monte Carlo. We impose a $\not\!\!E_T > 10$ GeV requirement to further reduce this background. A scale factor on the contribution from tridents is obtained from a control region with one or more jets and $\not\!\!E_T < 10$ GeV.

The expected and observed yields after these selection cuts have been applied are shown in Table V.

D. Trilepton Base Selection

In addition to the dilepton channel analyses, we search for potential Higgs signal in the trilepton final state. Trilepton events occur naturally in $WH \to WWW$ production, in the case where all three W bosons decay leptonically, and in $ZH \to ZWW$ production, where the Z boson and one of the W bosons from the Higgs decay leptonically while the second W boson decays hadronically. The gluon fusion and vector boson fusion production modes contribute to the trilepton final state only in cases where a photon or jet is misidentified as a lepton and are therefore not considered. The primary background in this search is WZ production, which also can result in a signature of three leptons and missing energy. In order to better determine the trilepton contributions from Drell-Yan events with a radiated photon, we use a sample of simulated $Z\gamma$ events. Direct WW and $W\gamma$ production give small contributions which are included within a common dilpeton plus fake (Z+jets) estimate.

The trilepton search is orthogonal to the dilepton searches, which require exactly two reconstructed leptons. The trilepton search requires three leptons which must not all have the same charge. At least one lepton is required to satisfy the trigger and have $E_T > 20$ GeV ($p_T > 20$ GeV/c) for electrons (muons). We loosen this requirement to > 10 GeV (GeV/c) for the second and third leptons to increase Higgs kinematic acceptance. To allow better

TABLE V: Expected and observed yields for background and signal for same-sign events with 1 or more jets in the final state. Only associated Higgs production with either a W or Z boson are considered as signal.

CDF Run II Preliminary $\int \mathcal{L} = 9.7$ fb^{-1}			
$M_H = 165$ GeV/c^2			
$t\bar{t}$	0.575	$\pm$	0.082
DY	16.4	$\pm$	4.6
WW	0.074	$\pm$	0.021
WZ	14.6	$\pm$	2.0
ZZ	2.43	$\pm$	0.33
W+jets	45	$\pm$	17
$W\gamma$	5.59	$\pm$	0.85
Total Background	85	$\pm$	18
WH	2.69	$\pm$	0.36
ZH	0.391	$\pm$	0.052
Total Signal	3.08	$\pm$	0.41
Data	87		

AllSB-SS

TABLE VI: Expected and observed yields for background and signal for trilepton events with a same-flavor opposite-sign dilepton pair in the Z-mass peak and one reconstructed jet. Only associated Higgs production with either a W or Z boson are considered as signal.

CDF Run II Preliminary $\int \mathcal{L} = 9.7$ fb^{-1}			
$M_H = 165$ GeV/c^2			
$t\bar{t}$	0.118	$\pm$	0.053
WZ	14.1	$\pm$	2.3
ZZ	5.81	$\pm$	0.83
Z+jets	9.9	$\pm$	2.3
$Z\gamma$	7.8	$\pm$	1.6
Total Background	37.7	$\pm$	4.6
WH	0.0437	$\pm$	0.0067
ZH	0.314	$\pm$	0.049
Total Signal	0.358	$\pm$	0.053
Data	38		

AllSB-trilepZ1j

discrimination against the dominant WZ background, events are separated into three channels depending on the number of reconstructed jets and whether or not there are two same-flavor (ee or $\mu\mu$) opposite-sign leptons with an invariant mass that falls within 10 GeV/c^2 of the 91 GeV/c^2 Z-boson mass.

Trilepton events with a same-flavor opposite-sign dilepton pair in the Z-mass peak have a Higgs signal contribution predominantly from ZH production. We require events of this type to have $\not\!\!E_T > 10$ GeV, a relatively loose selection criteria since ZH trilepton events must also contain a single high-p_T neutrino. The likely hadronic decay of the second W boson in ZH trilepton events results in the production of additional jets, so we also require events to have one or more reconstructed jets. In cases where we reconstruct two or more jets, we have access all of the Higgs decay products and can attempt to reconstruct the Higgs mass. For this reason, we separate events with one reconstructed jet and two or more reconstructed jets into two separate analysis channels. The expected and observed yields in these channels after applying selection cuts are shown in Tables VI and VII.

Trilepton events without a same-flavor opposite-sign dilepton pair in the Z-mass peak have a Higgs signal contribution predominantly from WH production. Because most WH trilepton events contain three neutrinos, they typically have high values of missing energy, and we therefore require events in this sample to have $\not\!\!E_T > 20$ GeV. However, WH trilepton events contain no jets at leading order, and we make no requirement on the number of reconstructed jets in these events. The expected and observed yields after these selection cuts have been applied are shown in Table VIII.

TABLE VII: Expected and observed yields for background and signal for trilepton events with a same-flavor opposite-sign dilepton pair in the Z-mass peak and two or more reconstructed jets. Only associated Higgs production with either a W or Z boson are considered as signal.

CDF Run II Preliminary	$\int \mathcal{L} = 9.7$ fb^{-1}	
$M_H = 165$ GeV/c^2		
$t\bar{t}$	0.163 ±	0.043
WZ	5.7 ±	1.3
ZZ	4.25 ±	0.89
Z+jets	7.8 ±	1.4
$Z\gamma$	2.96 ±	0.77
Total Background	20.9 ±	3.1
WH	0.0155 ±	0.0038
ZH	0.84 ±	0.12
Total Signal	0.86 ±	0.13
Data	26	

AllSB-trilepZ2j

TABLE VIII: Expected and observed yields for background and signal for trilepton events without a same-flavor opposite-sign dilepton pair in the Z-mass peak. Only associated Higgs production with either a W or Z boson are considered as signal.

CDF Run II Preliminary $\int \mathcal{L} = 9.7$ fb^{-1}		
$M_H = 165$ GeV/c^2		
$t\bar{t}$	0.75 ±	0.23
WZ	8.2 ±	1.2
ZZ	1.86 ±	0.26
Z+jets	4.9 ±	1.1
$Z\gamma$	4.87 ±	0.97
Total Background	20.6 ±	2.2
WH	1.03 ±	0.14
ZH	0.235 ±	0.032
Total Signal	1.27 ±	0.17
Data	20	

AllSB-trilepNoZ

V. DATA MODELING

The geometric and kinematic acceptance for the WW, WZ, ZZ, $W\gamma$, $Z\gamma$, Drell-Yan (DY), $t\bar{t}$, and all of the signal processes ($gg \to H$, WH, ZH, VBF) processes are determined using a Monte Carlo calculation of the collision followed by a GEANT3-based simulation of the CDF II detector [14] response. The Monte Carlo generator used for WW is MC@NLO [15], while for WZ, ZZ, DY, $t\bar{t}$, and the signal processes PYTHIA [16] is used. The $W\gamma$ and $Z\gamma$ processes are modeled with the generator described in [17]. We use the CTEQ5L parton distribution functions (PDFs) to model the momentum distribution of the initial-state partons [18].

A correction of up to 10% per lepton is applied to the simulation based on measurements of the lepton reconstruction and identification efficiencies in data using Z decays. An additional 10% correction based on $Z \to \ell\ell$ cross section measurements are applied to muons reconstructed from minimum ionizing energy deposits in the forward calorimeter to account for known poor modeling of the track reconstruction in this region. A 31% correction is applied to the $W\gamma$ background estimate, derived from the $W\gamma$ control region. In the opposite-sign two or more jet analysis, a scale factor of 1.058 is applied to the $t\bar{t}$ sample to account for the difference in efficiency between the data and simulation of the b-tag veto requirement. Trigger efficiencies are determined from $W \to e\nu$ data for electrons and from $Z \to \mu^+\mu^-$ data for muons.

The background from W+jets is estimated from a sample of events with an identified lepton and a jet that is required to pass loose isolation requirements and contain a track or energy cluster similar to those required in the lepton identification. The contribution of each event to the total yield is scaled by the probability that the jet is identified as a lepton. This probability is determined from multijet events collected with a set of jet-based triggers. A correction is applied for the small real lepton contribution using single W and Z boson Monte Carlo simulation. The background from Z+jets in the trilepton searches is estimated in a similar manner, using a sample of events with two identified leptons and a jet that is required to pass loose isolation requirements and contain a track or energy cluster similar to those required in the lepton identification.

In this analysis we consider contributions to the Higgs signal production from four sources. The gluon fusion cross section ($\sigma_{gg\to H}$) has been calculated to NNLL [3][4]. The calculations include two-loop electroweak effects and handling of the running b quark mass and are refinements of earlier NNLO calculations [19][20][21]. The electroweak corrections are computed in Refs. [22][23]. The technique of soft gluon resummation for this process was introduced in Ref. [24].

Associated Higgs (WH and ZH) [25][26][27][28] and vector boson fusion (VBF) Higgs production [25][29][30] are also considered. The Higgs boson decay branching ratio predictions are calculated in HDECAY version 3.53 [2]. Table IX gives the signal cross sections (in pb) and branching ratio for $H \to WW^*$ used in this analysis for each mass investigated.

VI. MULTIVARIATE DISCRIMINANTS

For each of the eight search channels, a NeuroBayes® neural network is trained on a weighted combination of known signal and background events from Monte Carlo independently for each of the 19 Higgs mass points. Each neural network has three layers consisting of input nodes, hidden nodes, and one output node. Once the neural network has been trained, templates are created for signal and background. For the zero and one jet channels, high S/B and low

TABLE IX: Cross sections for the signal processes considered in this analysis (given in *pb*) along with the branching ratio for $H \to WW$ for each Higgs mass investigated.

m_H (GeV)	$\sigma^{NNLL}_{gg\to H}$	σ_{WH}	σ_{ZH}	$\sigma_{\rm VBF}$	$\rm Br_{H\to WW}$
110	1.385	0.212	0.126	0.085	0.046
115	1.216	0.175	0.104	0.079	0.083
120	1.072	0.150	0.090	0.073	0.136
125	0.949	0.130	0.079	0.067	0.208
130	0.843	0.112	0.069	0.062	0.294
135	0.751	0.097	0.060	0.058	0.391
140	0.671	0.085	0.053	0.053	0.492
145	0.601	0.074	0.047	0.049	0.592
150	0.539	0.064	0.041	0.046	0.689
155	0.484	0.056	0.036	0.042	0.789
160	0.432	0.049	0.031	0.039	0.905
165	0.384	0.044	0.028	0.037	0.959
170	0.344	0.039	0.025	0.034	0.964
175	0.310	0.034	0.023	0.032	0.958
180	0.279	0.030	0.020	0.029	0.933
185	0.252	0.027	0.018	0.027	0.845
190	0.228	0.024	0.016	0.025	0.787
195	0.207	0.021	0.014	0.024	0.759
200	0.189	0.019	0.013	0.022	0.743

S/B templates based on the signal to background ratio of the different dilepton combinations are considered separately. Although this method acheives greater sensitivity than keeping all dilepton pairs in one cagetory, it was not done in the remaining channels due to low statistics. The templates are used as the final discriminant in calculating the 95% C.L. limits.

A. 0-jet Analysis

The 0-jet analysis uses nine input variables. The inputs are the ΔR between the leptons; the $\Delta\phi$ between the leptons; the transverse momentum of the leading lepton; the transverse momentum of the subleading lepton; the scalar sum of the transverse energies of leptons and the $\not{E}_T$ ($H_{\rm T}$), the transverse mass of the vector sum of the lepton momenta and the $\not{E}_T$ ($M_T(ll\not{E}_T)$); the likelihood ratio for Higgs to WW production (LR_{HWW}); the likelihood ratio for WW production (LR_{WW}); and the invariant mass of the two leptons ($M_{\ell\ell}$). The likelihood variables were produced using an event-by-event calculation of the probability density $P_m(x_{obs})$. Five modes (m) are modeled including WW, ZZ, $W\gamma$, W+jet, and $H \to WW$ (for all 19 masses). The probability density for any given mode m is given by:

$$P_m(x_{obs}) = \frac{1}{<\sigma_m>} \int \frac{d\sigma_m^{th}(y)}{dy} \epsilon(y) G(x_{obs}, y) dy \tag{1}$$

where

x_{obs}	are the observed "leptons" and $\vec{\not{E}}_T$,
y	are the true lepton four-vectors (including neutrinos),
σ_m^{th}	is the leading-order theoretical calculation of the cross-section for mode m,
$\epsilon(y)$	is the total event efficiency $\times$ acceptance,
$G(x_{obs}, y)$	is an analytic model of resolution effects, and
$\frac{1}{<\sigma_m>}$	is the normalization.

The function $\epsilon(y)$ describes the probabilities of a parton level object (e, μ, γ, or parton) to be reconstructed as one of the lepton categories. The efficiency function is determined solely from Monte Carlo for e and μ but comes from a combination of Monte Carlo and data-driven measurements described in Section V for γ and partons. The event probability densities are used to construct a discriminant:

$$LR_S(x_{obs}) \equiv \frac{P_S(x_{obs})}{P_S(x_{obs}) + \Sigma_i k_i P_i(x_{obs})},$$

where S is either WW or $H \to WW$, k_i is the expected fraction for each background and $\Sigma_i k_i = 1$.

Because of the missing neutrinos in the final state, the integral in Equation 1 integrates out the unobserved degrees of freedom (DOF) reducing the 12 DOF in y to the eight measured DOF. Distributions of the nine neural network input variables with the expected and observed yields for signal and background are shown in Fig. 1. The NN output templates are shown in Fig. 2 for $m_H = 160$ GeV/c^2.

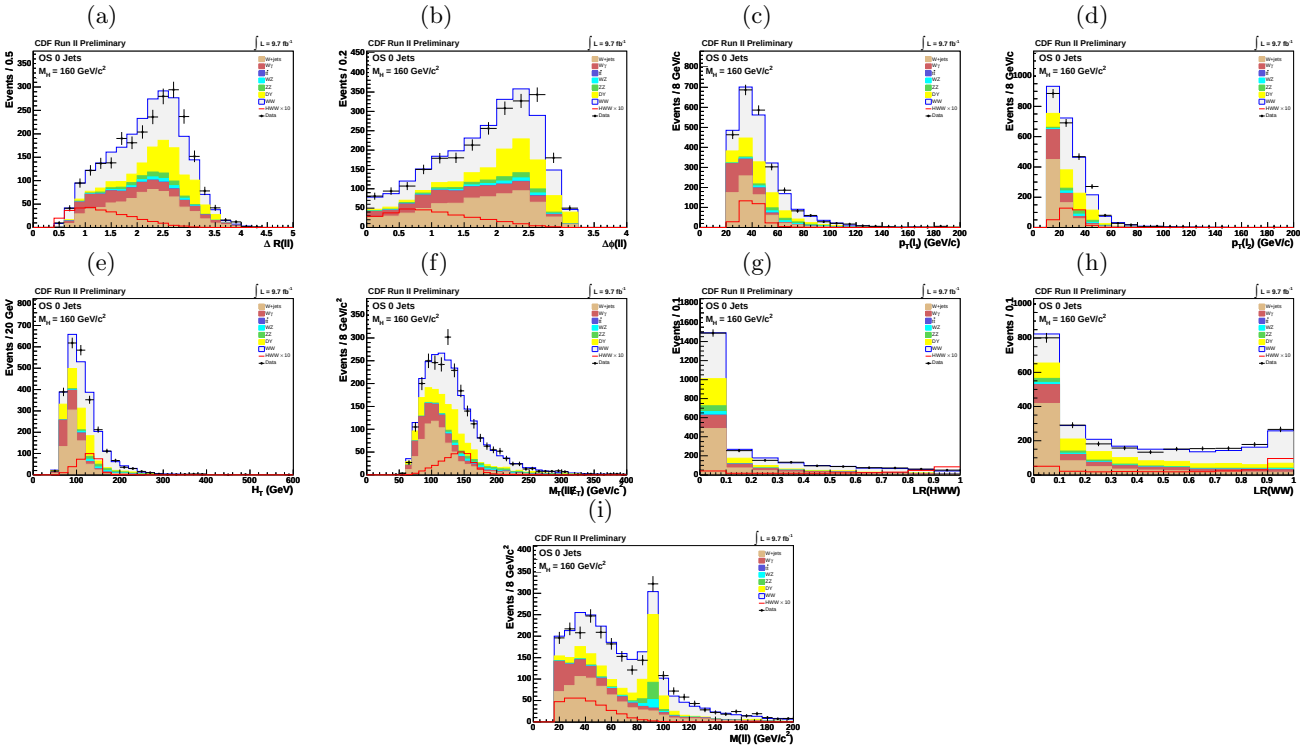

FIG. 1: Distributions of input variables to the neural network for opposite-sign dilepton events with zero jets in the final state: (a) ΔR separation of leptons (b) $\Delta\phi$ separation of leptons (c) leading lepton p_T (d) subleading lepton p_T (e) $H_{\rm T}$ (f) $M_T(ll\not{E}_T)$ (g) LR_{HWW} (h) LR_{WW} (i) $M_{\ell\ell}$.

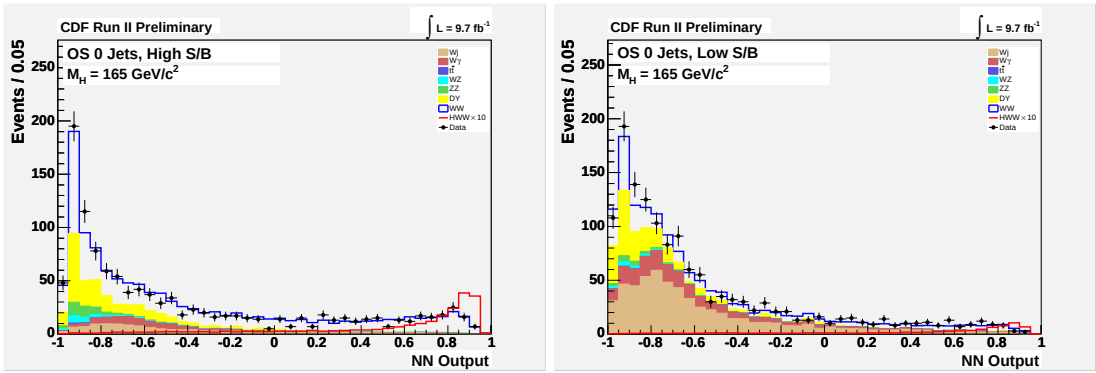

FIG. 2: Neural network templates for high S/B (*left*) and low S/B (*right*) for $m_H = 165$ GeV/c^2 for opposite-sign dilepton events with zero jets.

B. 1-jet Analysis

The 1-jet analysis uses twelve input variables. The inputs are $M_{\ell\ell}$; $M_T(ll\not{E}_T)$; the ΔR between the leptons; $H_{\rm T}$; $\not{E}_{T_{\rm spec}}$; the p_T of the leading lepton; the p_T of the subleading lepton; the energy of the leading lepton; the centrality; the cosine of $\Delta\phi$ between the leptons in the CM frame; the $\Delta\phi$ between $\not{E}_T$ and the nearest lepton or jet; and the $\not{E}_T$ significance. Distributions of these variables with expected and observed yields for signal and background are shown in Fig. 3. The NN output templates are shown in Fig. 4 for $m_H = 160$ GeV/c^2.

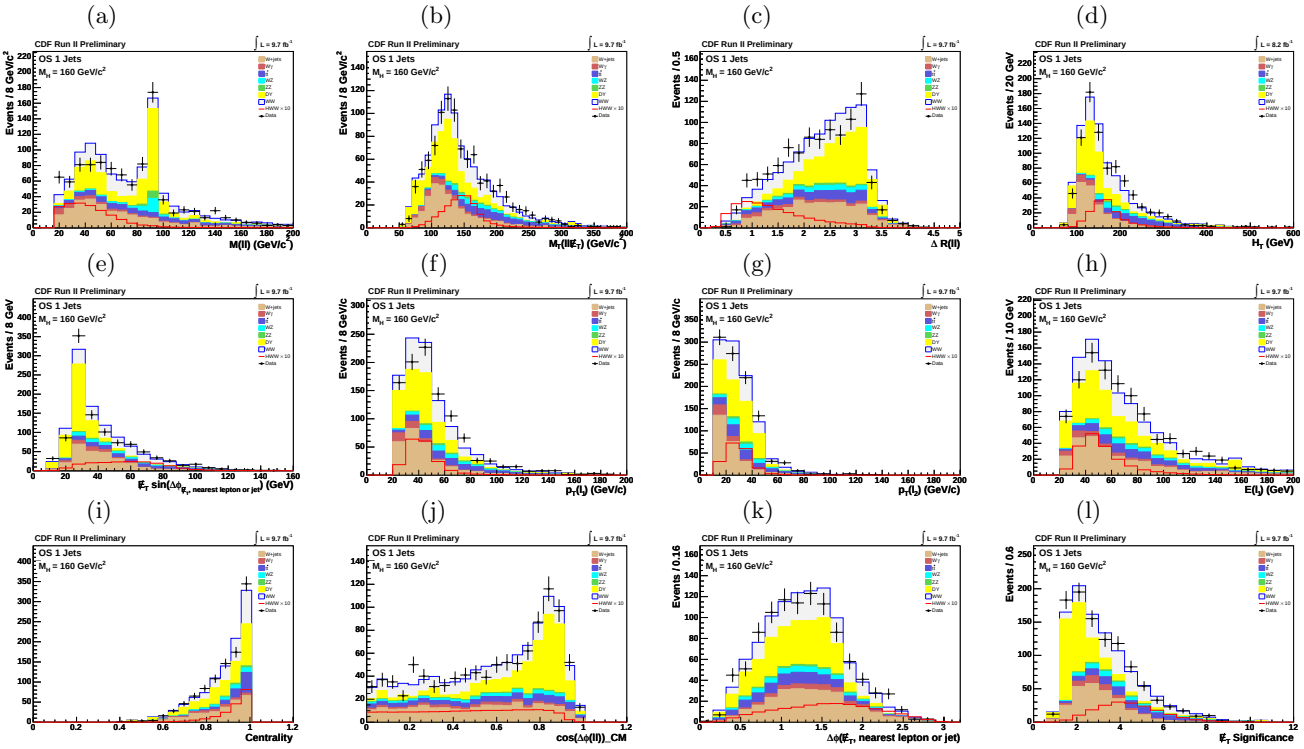

FIG. 3: Distributions of input variables to the neural network for opposite-sign dilepton events with one jet in the final state: (a) $M_{\ell\ell}$ (b) $M_T(ll\not{E}_T)$ (c) ΔR separation of leptons (d) $H_{\rm T}$ (e) $\not{E}_{T_{\rm spec}}$ (f) leading lepton p_T (g) subleading lepton p_T (h) leading lepton energy (i) centrality (j) $\cos(\Delta\phi)_{CM}$ (k) $\Delta\phi(\not{E}_T, nearestleptonorjet)$ (l) $\not{E}_T$ significance

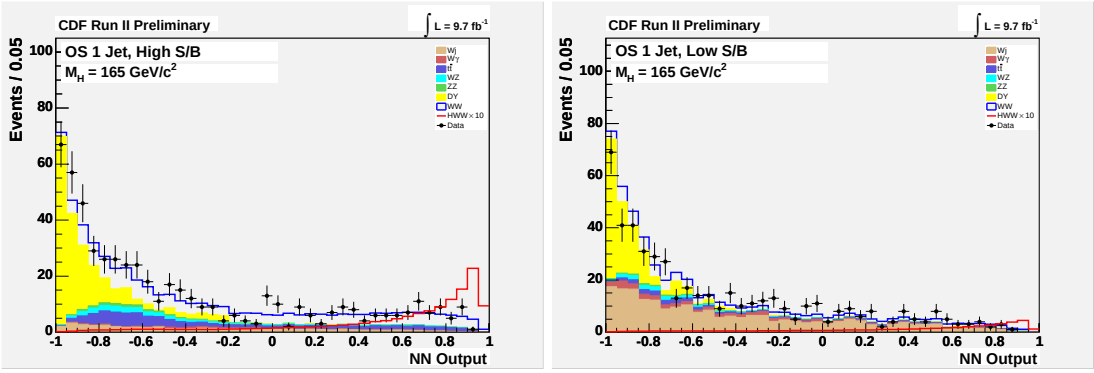

FIG. 4: Neural network templates for high S/B (*left*) and low S/B (*right*) for $m_H = 165$ GeV/c^2 for opposite-sign dilepton events with one jet.

C. 2-jet Analysis

The 2-jet analysis uses eight input variables. The inputs are $M_{\ell\ell}$; the p_T of the leading lepton; the p_T of the subleading lepton; $H_{\rm T}$; the ΔR between the leptons; the $\Delta\phi$ between the leptons; the $\Delta\phi$ between the vector sum of lepton momenta and the $\not\!\!E_T$ ($\Delta\phi(\ell\ell, \not\!\!E_T)$); and the magntiude of the vector sum of the transverse momenta of the first and second jets ($p_T(j_1 j_2)$). Distributions of these variables with expected and observed yields for signal and background are shown in Fig. 5. The NN output template is shown in Fig. 6 for $m_H = 160$ GeV/c^2.

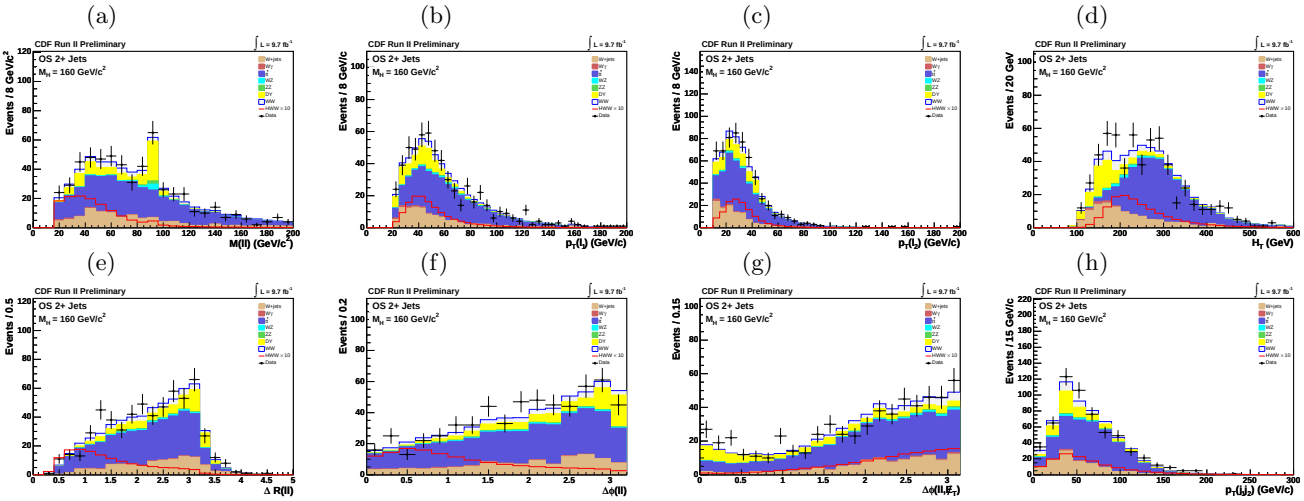

FIG. 5: Distributions of input variables to the neural network for opposite-sign dilepton events with two or more jets in the final state: (a) $M_{\ell\ell}$ (b) leading lepton $p_{\rm T}$ (c) subleading lepton $p_{\rm T}$ (d) $H_{\rm T}$ (e) ΔR separation of leptons (f) $\Delta\phi$ separation of leptons (g) $\Delta\phi(\ell\ell, \not\!\!E_T)$ (h) $p_T(j_1 j_2)$.

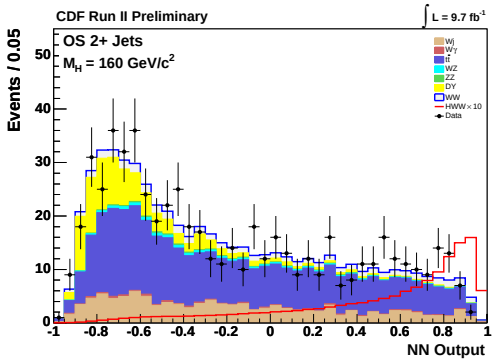

FIG. 6: Neural network template for $m_H = 160$ GeV/c^2 for opposite-sign dilepton events with two or more jets.

D. Low $M_{\ell\ell}$ Analysis

The low $M_{\ell\ell}$ analysis uses thirteen input variables. The inputs are the p_T of the leading lepton; the energy of the leading lepton; the p_T of the subleading lepton; the energy of the subleading lepton; the scalar sum of the transverse energies of the leptons and the $\not\!\!E_T$; $\Delta\phi(\ell\ell, \not\!\!E_T)$; the $\not\!\!E_T$ significance based on the sum of lepton and jet energies ($\not\!\!E_T/\sqrt{\Sigma E_{\rm T}(\text{leptons, jets})}$); $\not\!\!E_{T\,\rm spec}$; ΔR between the leptons; $\Delta\phi$ between the leptons; $H_{\rm T}$; the scalar sum of lepton and jet (if any) transverse energies; and the magnitude of the vector sum of lepton and jet (if any) transverse energies. Distributions of these variables with expected and observed yields for signal and background are shown in Fig. 7. The NN output template is shown in Fig. 8 for $m_H = 160$ GeV/c^2.

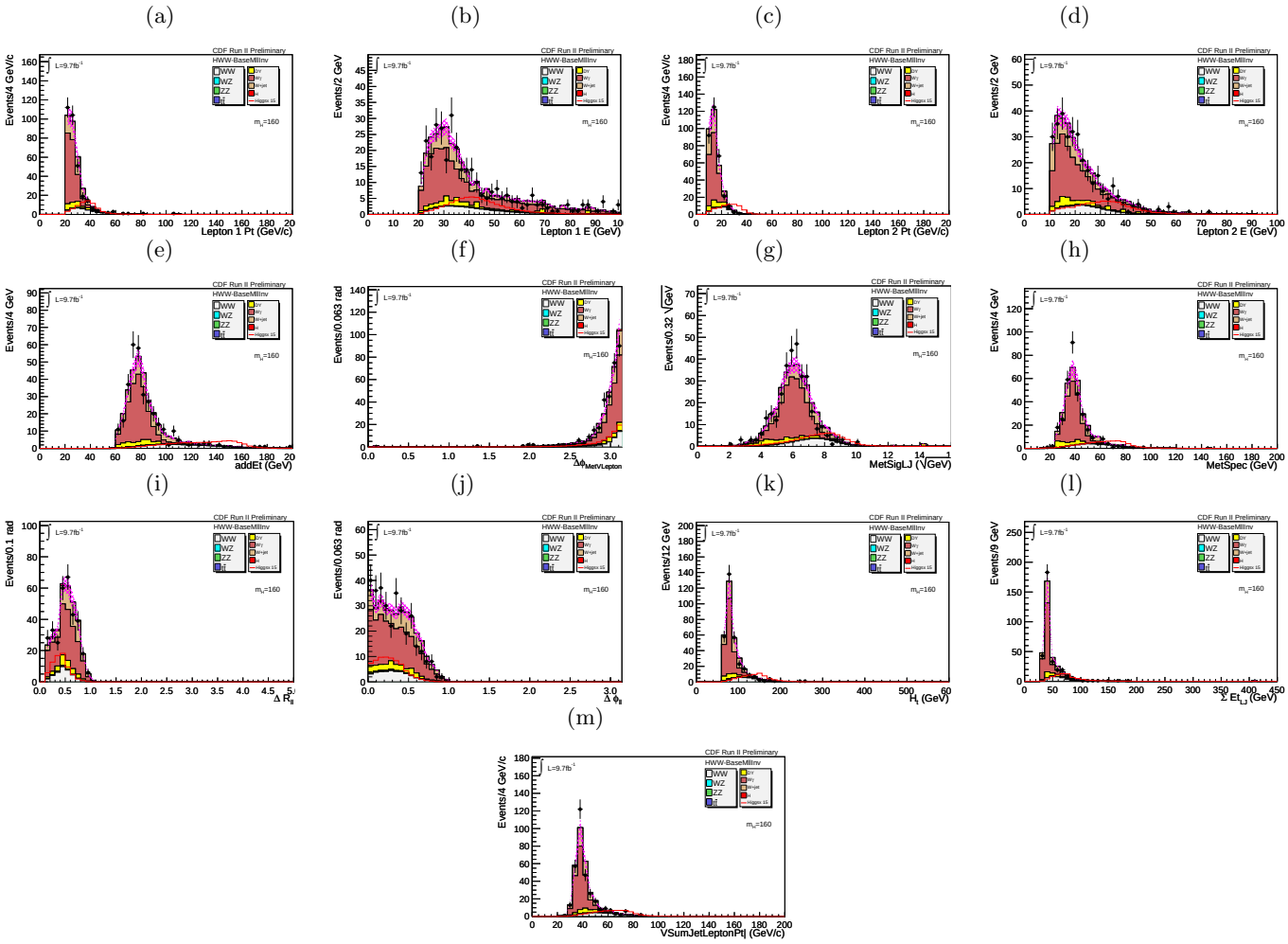

FIG. 7: Distributions of input variables to the neural network for opposite-sign dilepton events with $M_{\ell\ell} < 16$ GeV/c^2 and zero or one jets in the final state: (a) leading lepton $p_{\rm T}$ (b) leading lepton energy (c) subleading lepton $p_{\rm T}$ (d) subleading lepton energy (e) sum of transverse energies of leptons and the $\not\!\!E_T$ (f) $\Delta\phi(\ell\ell, \not\!\!E_T)$ (g) $\not\!\!E_T/\sqrt{\Sigma E_{\rm T}(\text{leptons, jets})}$ (h) $\not\!\!E_{T_{\rm spec}}$ (i) ΔR separation of leptons (j) $\Delta\phi$ separation of leptons (k) $H_{\rm T}$ (l) sum of transverse energies of leptons and jets (m) magnitude of vector sum of transverse energies of leptons and jets.

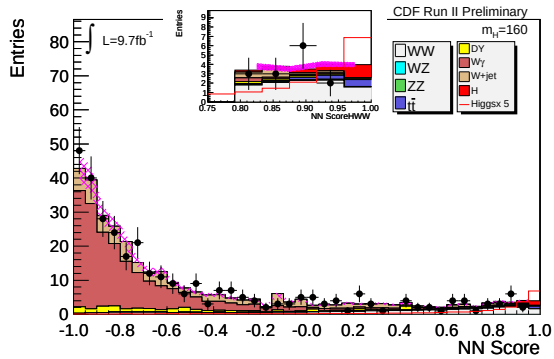

FIG. 8: Neural network template for $m_H = 160$ GeV/c^2 for opposite-sign dilepton events with $M_{\ell\ell} < 16$ GeV/c^2 and zero or one jets.

E. Same-Sign Analysis

The same-sign analysis uses nine input variables. The inputs are the number of reconstructed jets; the $\not\!\!E_T$ significance based on the sum of all energy in the calorimeter ($\not\!\!E_T/\sqrt{\Sigma E_{\rm T}}$); the scalar sum of the transverse energies of all jets; $\not\!\!E_{T_{\rm spec}}$; the transverse energy of the leading jet; the transverse momenta of the leading and the subleading leptons; and the $\Delta\phi$ between the $\not\!\!E_T$ and the closest lepton or jet ($\Delta\phi(\not\!\!E_T, \text{nearest lepton or jet})$). Distributions of these variables with expected and observed yields for signal and background are shown in Fig. 9. The NN output template is shown in Fig. 10 for $m_H = 165$ GeV/c^2.

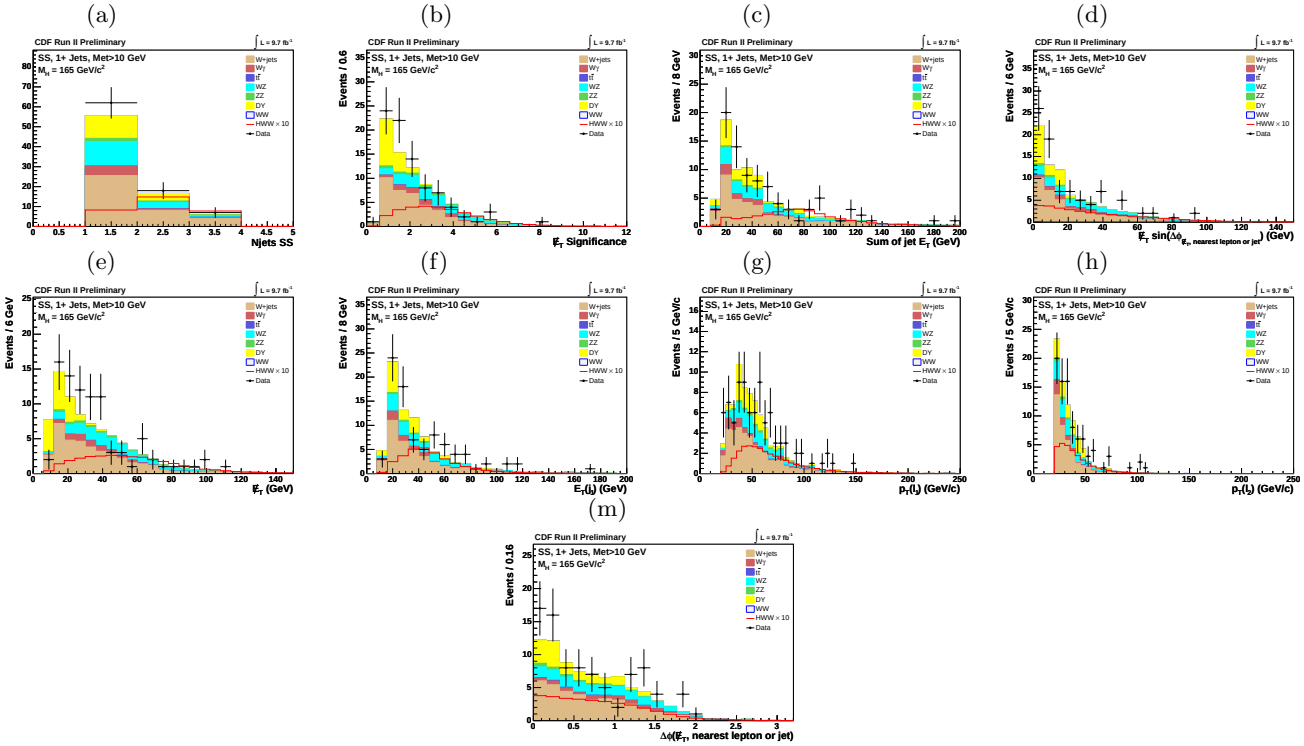

FIG. 9: Distributions of input variables to the neural network for same-sign dilepton events with one or more jets: (a) number of reconstructed jets (b) $\not\!\!E_T/\sqrt{\Sigma E_{\rm T}}$ (c) $\Sigma E_{\rm T}$(jets) (d) $\not\!\!E_{T_{\rm spec}}$ (e) $\not\!\!E_T$ (f) leading jet $E_{\rm T}$ (g) leading lepton $p_{\rm T}$ (h) subleading lepton $p_{\rm T}$ (i) $\Delta\phi(\not\!\!E_T, \text{nearest lepton or jet})$.

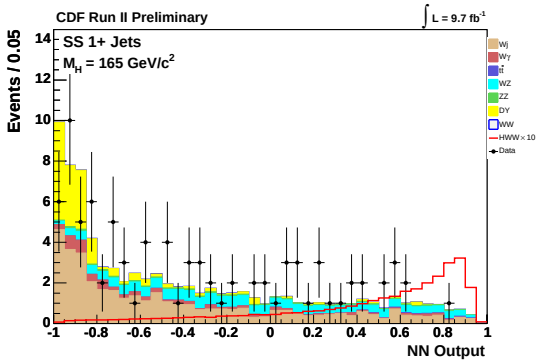

FIG. 10: Neural network template for $m_H = 165$ GeV/c^2 for same-sign dilepton events with one or more jets.

F. Trilepton Analyses

Three different sets of discriminating variables are used for the trilepton search channels. For the channels that contain events with a same-flavor opposite-sign dilepton pair in the Z-boson mass window, we take advantage of the fact that we have "tagged" the two leptons coming from the Z-boson decay and can associate the third as coming from a W-boson decay in constructing our input variables. In the case of events with one reconstructed jet and a same-flavor opposite-sign dilepton pair, we use sixteen neural network input variables which are $\not\!\!E_T$; the ΔR between the leading jet and the lepton from W-boson decay; the leading jet E_T; the ΔR between the closest pair of opposite-sign leptons; the $\Delta\phi$ between the lepton from the W-boson decay and the $\not\!\!E_T$; the $\Delta\phi$ between the vector sum of the lepton momenta and the $\not\!\!E_T$; the ΔR between the furthest pair of opposite-sign leptons; the invariant mass of the three leptons; the transverse mass of the vector sum of all leptons and jets and the $\not\!\!E_T$; the transverse mass of the reconstructed Higgs, the $\Delta\phi$ between the subleading lepton and the $\not\!\!E_T$; the three-lepton flavor combination; the invariant mass of the subsubleading lepton and all jets and the $\not\!\!E_T$; $H_{\rm T}$; the invariant mass of the lepton from the W-boson decay and the $\not\!\!E_T$; and the transverse mass of the lepton from the W-boson decay and the $\not\!\!E_T$. Distributions of these variables with expected and observed yields for signal and background are shown in Fig. 11. The NN output template is shown in Fig. 12 for $m_H = 160$ GeV/c^2.

In the case of events with two or more reconstructed jets and and a same-flavor opposite-sign dilepton pair in the Z-boson mass window, we take advantage of the fact that all Higgs decay products are available within the event to "reconstruct" the mass of the Higgs. The ten neural network input variables used for this channel are the ΔR between the lepton from W-boson decay and the closest jet; the invariant mass of the two leading E_T jets; the reconstructed mass of the W-boson with the leptonic decay; $\not\!\!E_T$; the ΔR between the reconstructed W-bosons; the leading jet E_T; the subleading jet E_T; the transverse mass of the lepton from the W-boson decay and the $\not\!\!E_T$; the transverse mass of the reconstructed Higgs, and the three-lepton flavor combination. Distributions of these variables with expected and observed yields for signal and background are shown in Fig. 13. The NN output template is shown in Fig. 14 for $m_H = 160$ GeV/c^2.

For the analysis of trilepton events without a same-flavor opposite-sign dilepton pair in the Z-boson mass window we use fourteen neural input variables which are the transverse mass of the subsubleading p_T lepton and the $\not\!\!E_T$; the ΔR between the closest pair of opposite-sign leptons; the three-lepton flavor combination; the invariant mass of the closest pair of opposite-sign leptons, the ΔR between the furthest pair of opposite-sign leptons, $H_{\rm T}$, the transverse mass of all leptons; the transverse mass of the vector sum of all leptons and jets and the $\not\!\!E_T$; the invariant mass of the subsubleading p_T lepton, all jets, and the $\not\!\!E_T$; the $\Delta\phi$ between the subleading p_T lepton and the $\not\!\!E_T$; the subleading lepton p_T; $\not\!\!E_T$; the number of reconstructed jets; and the invariant mass of the leading p_T lepton, the subleading p_T lepton, and the $\not\!\!E_T$. Distributions of these variables with expected and observed yields for signal and background are shown in Fig. 15. The NN output template is shown in Fig. 16 for $m_H = 160$ GeV/c^2.

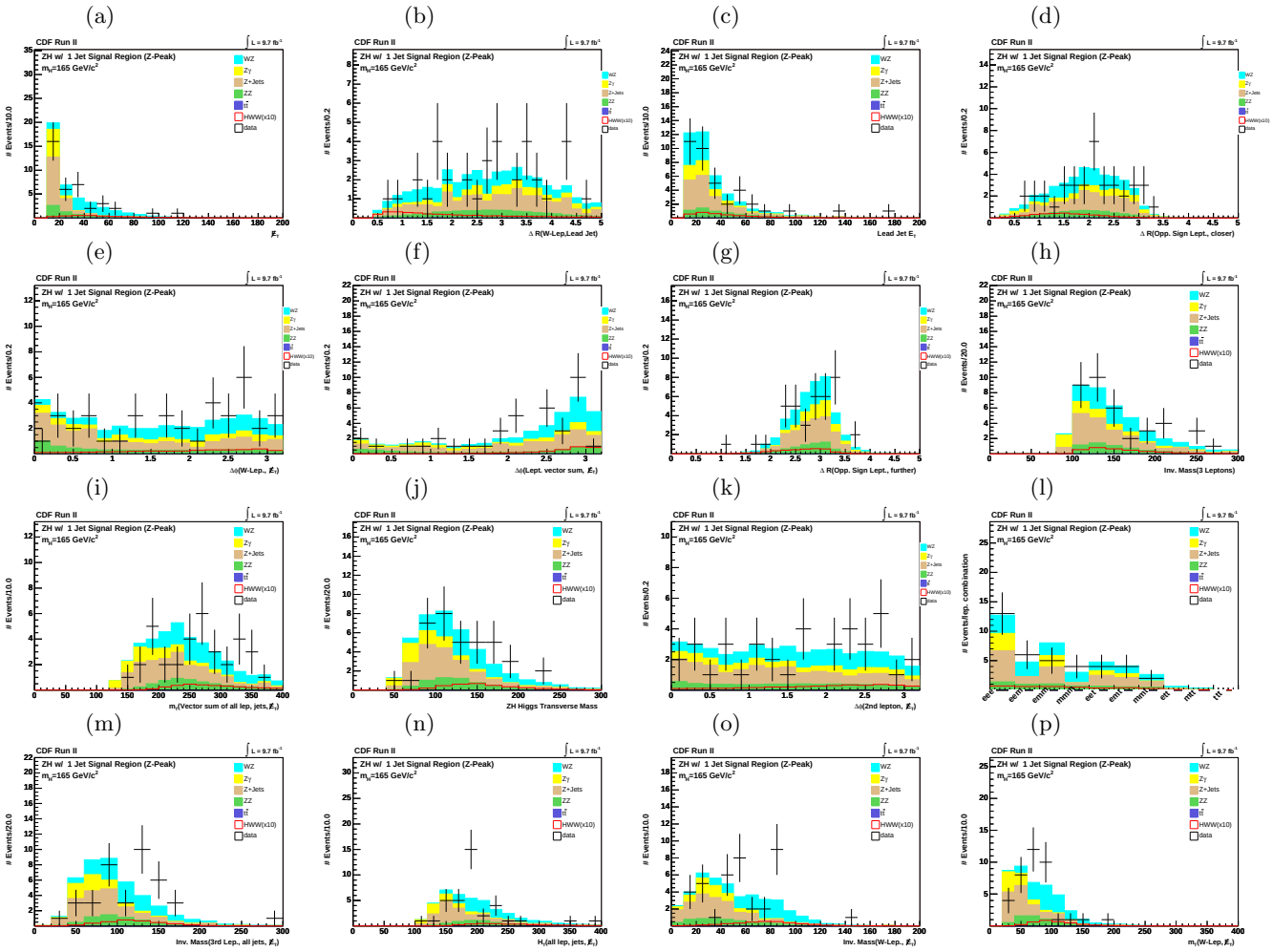

FIG. 11: Distributions of input variables to the neural network for trilepton events with a same-flavor opposite-sign dilepton pair in the Z-mass peak and one reconstructed jet: (a) $\not\!\!E_T$ (b) ΔR separation of leading jet and W-lepton (c) leading jet $E_{\rm T}$ (d) ΔR separation of closest opposite-sign leptons (e) $\Delta\phi$ separation of $\not\!\!E_T$ and W-lepton (f) $\Delta\phi$ separation of $\not\!\!E_T$ and vector sum of three leptons (g) ΔR separation of furthest opposite-sign leptons (h) trilepton invariant mass (i) $M_{\rm T}$ of vector sum of all leptons and jets and the $\not\!\!E_T$ (j) transverse mass of the reconstructed Higgs (k) $\Delta\phi$ separation of subleading lepton and $\not\!\!E_T$ (l) three lepton flavor combination (m) invariant mass of subsubleading lepton, all jets, and the $\not\!\!E_T$ (n) $H_{\rm T}$ (o) invariant mass of the $\not\!\!E_T$ and W-lepton (p) $M_{\rm T}$ of the $\not\!\!E_T$ and W-lepton.

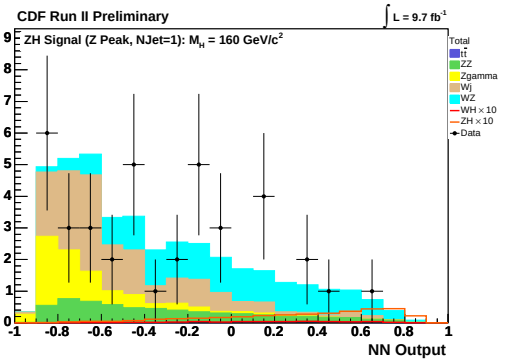

FIG. 12: Neural network template for $m_H = 160$ GeV/c^2 for trilepton events with one reconstructed jet and a same-flavor opposite-sign dilepton pair in the Z-mass peak.

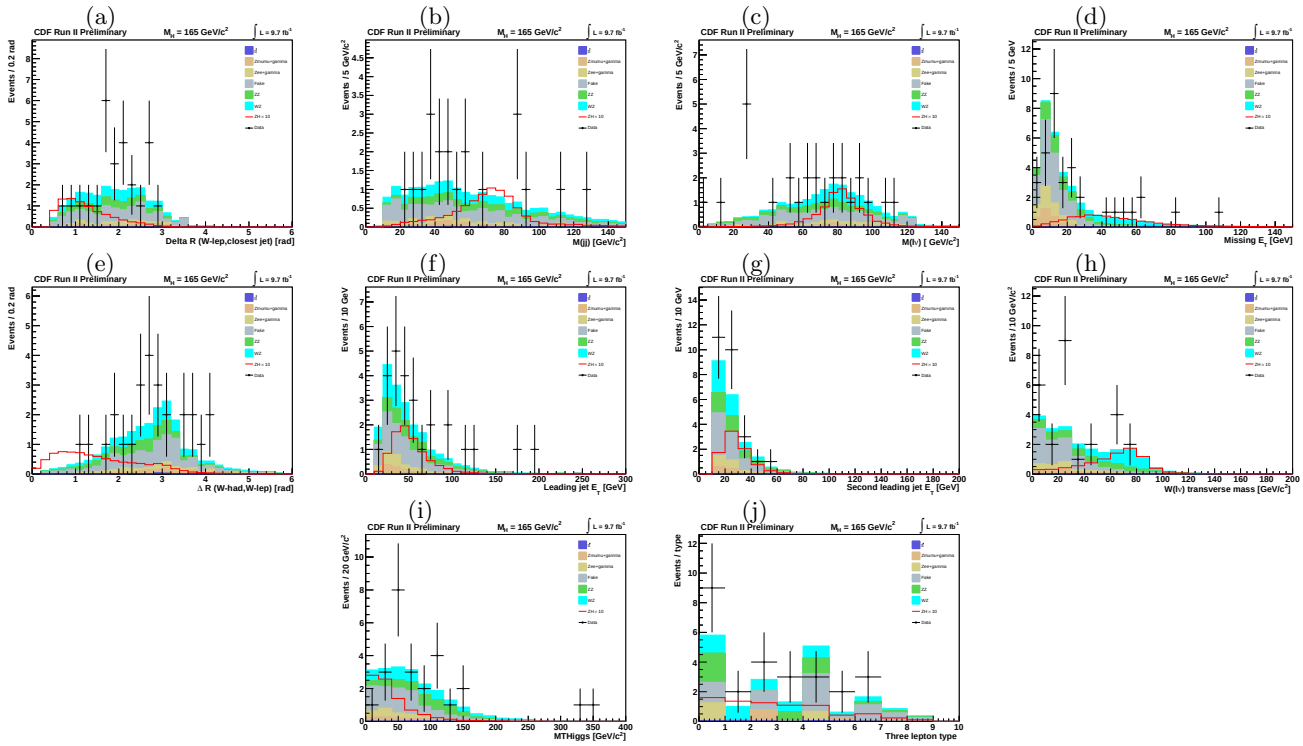

FIG. 13: Distributions of input variables to the neural network for trilepton events with a same-flavor opposite-sign dilepton pair in the Z-mass peak and two or more reconstructed jets: (a) ΔR separation of W-lepton and closest jet (b) invariant mass of two leading E_{T} jets (c) reconstructed mass of W-boson with leptonic decay (d) $\not\!\!E_T$ (e) ΔR separation of reconstructed W bosons (f) leading jet E_{T} (g) subleading jet E_{T} (h) M_{T} of the $\not\!\!E_T$ and W-lepton (i) transverse mass of the reconstructed Higgs (j) three lepton flavor combination.

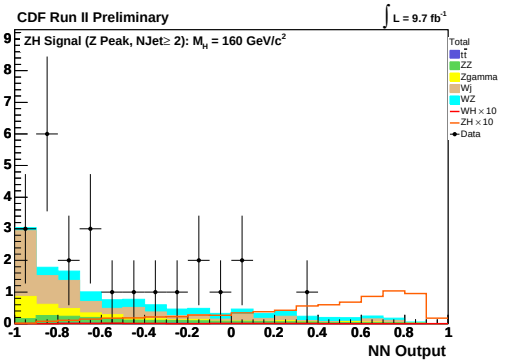

FIG. 14: Neural network template for $m_H = 160$ GeV/c^2 for trilepton events with two or more reconstructed jets and a same-flavor opposite-sign dilepton pair in the Z-mass peak.

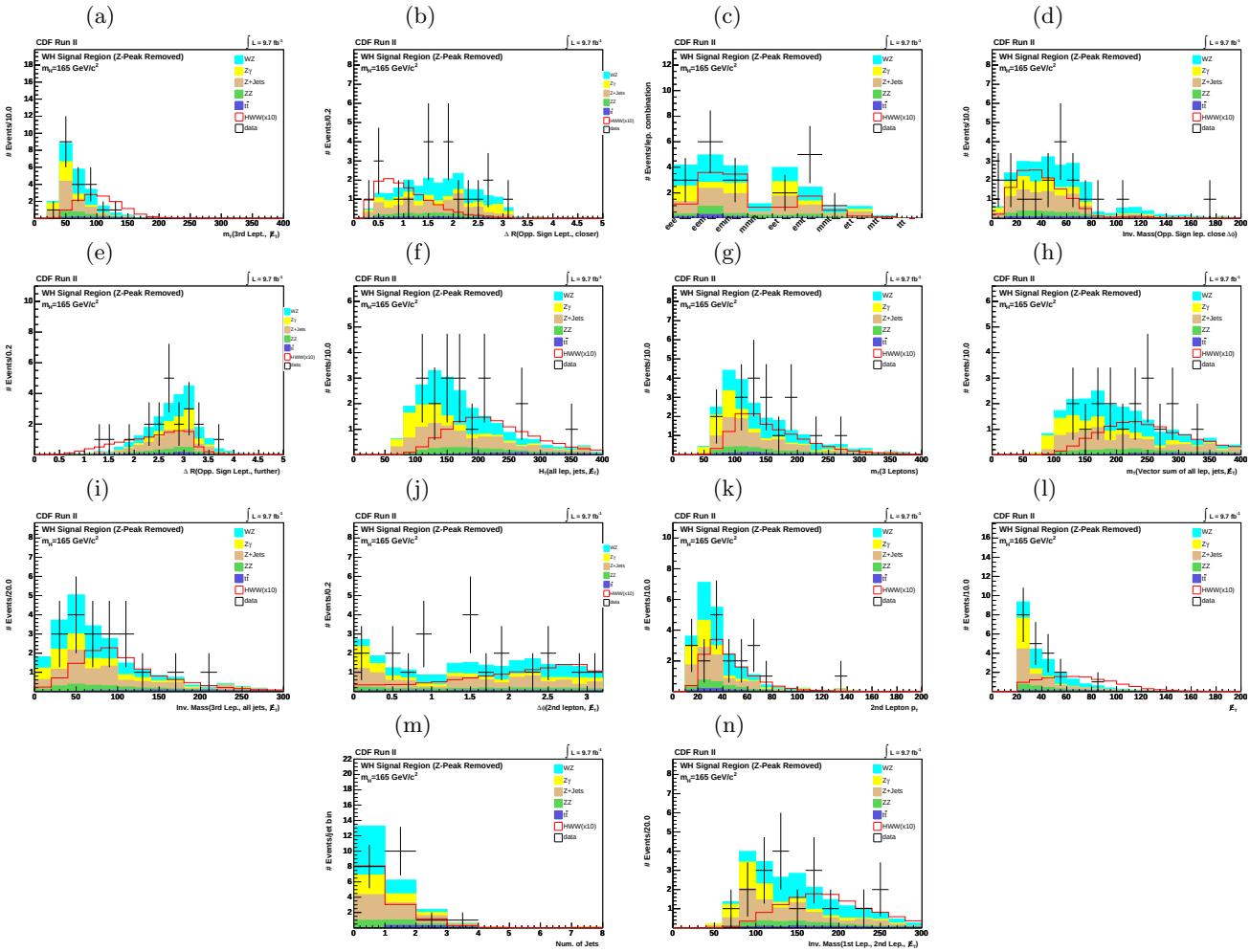

FIG. 15: Distributions of input variables to the neural network for trilepton events without a same-flavor opposite-sign dilepton pair in the Z-mass peak: (a) M_{T} of subsubleading lepton and the $\not\!\!E_T$ (b) ΔR separation of closest opposite-sign leptons (c) three lepton flavor combination. (d) invariant mass of closest opposite-sign leptons (e) ΔR separation of furthest opposite-sign leptons (f) H_{T} (g) M_{T} of all leptons (h) M_{T} of vector sum of all leptons and jets and the $\not\!\!E_T$ (i) invariant mass of subsubleading lepton, all jets, and the $\not\!\!E_T$ (j) $\Delta\phi$ separation of subleading lepton and the $\not\!\!E_T$ (k) subleading lepton p_{T} (l) $\not\!\!E_T$ (m) number of reconstructed jets (n) invariant mass of leading and subleading leptons and the $\not\!\!E_T$.

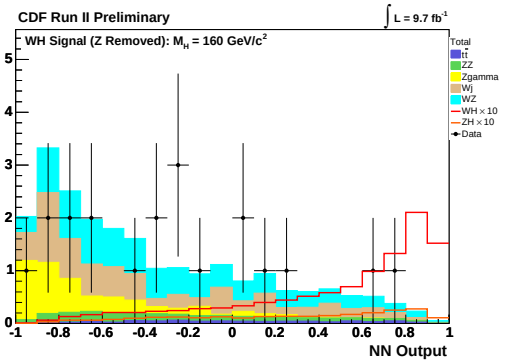

FIG. 16: Neural network template for $m_H = 160$ GeV/c^2 for trilepton events without a same-flavor opposite-sign dilepton pair in the Z-mass peak.

VII. SYSTEMATICS

Systematic uncertainties associated with the Monte Carlo simulation affect the Higgs, WW, WZ, ZZ, $W\gamma$, $Z\gamma$, DY, and $t\bar{t}$ acceptances taken from the simulated event samples. Uncertainties originating from lepton selection and trigger efficiency measurements are propagated through the acceptance calculation leading to a 4.3% uncertainty on the predicted signal and background event yields. For the same-sign channel, we assign an additional systematic to the predicted backgrounds which result solely from lepton charge mismeasurements(WW, $t\bar{t}$, and DY). In these cases the assigned uncertainty is one-half of the difference between measured lepton charge mismeasurement rates in data and Monte Carlo.

We also assign acceptance uncertainties due to potential contributions from higher-order effects. In the case of our WW background model, we run the next-to-leading order (MC@NLO [15]) generator used to create our simulated event samples with different choices for the scales and PDF input model [31] used in the calculation and determine uncertainties based on changes in the observed acceptance. In the case of other backgrounds, which are simulated only at leading order, we assign the full difference in the observed acceptance for WW between leading order (PYTHIA-based [16]) and next-to-leading order (MC@NLO [15]) which is 10%. The largest uncertainty on the Drell-Yan background originates from modeling of the fake missing E_T in these events. Our Drell-Yan modeling is tuned using candidate events with intermediate $\not{E}_T$ (values just below the lower threshold for selecting events in our signal region). An additional 20% uncertainty is applied to the predicted Drell-Yan event yields based on a range of variations in our tuning parameters consistent with the observed data. The uncertainty in the Boson Radiation prediction is taken from the 9.2 % statistical error on the data comparison in the low $M_{\ell\ell}$ control region defined by $15 < \not{E}_{T\,\mathrm{spec}} < 25$. We also vary the jet energy scale up and down within one standard deviation to determine effects on acceptance individually for each channel. The uncertainties taken for these effects are often anti-correlated between different channels since the typical effect of changes in jet energy scale is to move events from one channel to another.

For the $W\gamma$ background contributions, there is an additional uncertainty of 10% due to the detector material description and conversion veto efficiency. We measure a scale factor from data using a control sample of same-sign events satisfying the other selection cuts for our low $M_{\ell\ell}$ signal region. The residual uncertainty is based on the statistics of this control sample and uncertainties on the small non-$W\gamma$ background contribution. We assign an additional acceptance uncertainty on our extrapolation of this measured scale factor from the low $M_{\ell\ell}$ control region to the other dilepton signal regions. For the low $M_{\ell\ell}$ analysis, the $W\gamma$ computation is done using MadGraph4 [13] and the systematic uncertainty of 8.4% is used based on the statistical accuracy of the data. The systematic uncertainties on our W+jets and Z+jets background predictions are taken from differences in the measured probabilities for a jet to be identified as a lepton using jet data collected using four different jet E_T trigger thresholds. These variations correspond to changing the parton composition of the jets and the relative amount of contamination from real leptons.

The uncertainties on the $WW/WZ/ZZ$ and $t\bar{t}$ cross sections are assigned to be 6% [32] and 7% [33][34][35], respectively. In addition, all signal and background estimates obtained from simulation have an additional 5.9% uncertainty originating from the luminosity measurement [36].

Most systematic uncertainties on the signal processes are assessed using the same techniques described for the background processes. Uncertainties on the theoretical cross sections vary for the different Higgs production mechanisms. Associated production cross sections are known to NNLO, so the theoretical uncertainty on these cross sections is small, less than 5% [37]. Vector Boson Fusion (VBF) production is known only to NLO, so the residual theoretical uncertainty is higher (on the order of 10% [37]). Gluon fusion is a QCD process, so although it is known to NNLO, the corresponding theoretical uncertainty is still significant. We use recent studies with the HNNLO program [38][39][40] to assign theoretical uncertainties based on observed changes in the cross section originating from modications to the renormalization and factorization scales used in the calculation and the input PDF model. In the case of PDF model uncertainties, we use MSTW 2008 NNLO PDF set [31] eigenfunctions, which also account for potential variations originating from uncertainty in the value of $\alpha_s(q^2)$. Since we separate events into different analysis channels based on jet multiplicity, these uncertainties are separately determined for each channel [41][42].

To evaluate potential shape uncertainties associated with our gluon fusion Higgs signal templates, we vary our default choice for the Higgs p_T spectrum in our simulated event sample, which is obtained from the HqT program [43][44], using re-weighting functions determined from RESBOS [45][46][47]. The re-weighting functions are based on shape differences between the RESBOS Higgs p_T spectra obtained using our default scale choice and those obtained using higher and lower (by a factor of two) scale choices. We re-weight the simulated signal events to match at generator-level the modified Higgs p_T spectra and study the effect on the shape of our final signal templates. We do not consider changes in the signal yield obtained from this procedure as additional rate uncertainties since the corresponding acceptance effects are already included within the previously assigned cross section uncertainties originating from scale choice.

The complete set of systematic uncertainties are summarized in Tables XXI- XXIII for the main opposite-sign lepton channels; Table XXIV for the opposite-sign lepton, low $M_{\ell\ell}$ channel; Table XXV for same-sign lepton channel;

and Tables XXVI- XXVIII for the trilepton channels.

VIII. CROSS-CHECKS

We use several control regions, described below, to validate various aspects of our data modeling. The sample sizes of the control regions are designed to be large enough to give statistically meaningful tests.

A $W\gamma$ control sample is constructed by requiring same-sign events with the low $M_{\ell\ell}$ selection described in Section IV B. As described previously this control region is used to extract a scale factor that is applied to our simulated event yields for the $W\gamma$ background to correct for differences in the detector material description and conversion veto efficiencies between data and Monte Carlo. The predicted and observed yields for this control region (prior to applying the $W\gamma$ scale factor to the predicted yields) are shown in Table XIV.

A second model for $W\gamma$ based on MadGraph4 was used only in the low $M_{\ell\ell}$ analysis. The SS low Mll control region shows excellent agreement and no correction factor is applied in the low Mll analysis. The predicted and observed yields for this control region for the MadGraph4 are shown in Table XV.

A $t\bar{t}$ control sample is constructed using the default candidate selection in Section IV A making a requirement of two or more jets in the event and reversing the b-tag veto requirement such that only events with one or more jets identified as originating from a b quark are accepted. We observe good agreement between data and the estimate based on our theoretical prediction for the $t\bar{t}$ cross-section. The predicted and observed yields are shown in Table XVII.

A W+jets control sample is constructed from events with no reconstructed jets using the same-sign event selection described in Section IV C. This control sample contains contributions primarily from jets misidentified as leptons, with additional contributions from photon conversions and real lepton charge misidentifications. The predicted and observed yields for this control region are shown in Table XVIII.

We use two control regions to test our Drell-Yan modeling. Our inclusive Drell-Yan sample (selected using no $\not\!\!E_T$ requirements) provides a high statistics test of the simulated acceptances, measured scale factors, and measured trigger efficiencies for each of the lepton types used in our searches. The predicted and observed yields for this control region are shown in Table XIX. A second control sample selected using intermediate $\not\!\!E_T$ cuts is used to tune the modeling of $\not\!\!E_T$ in our simulated event sample. This second Drell-Yan control sample is constructed using the default candidate selection in Section IV A with the exception of requiring $15 < \not\!\!E_{T\mathrm{spec}} < 25$ GeV instead of $\not\!\!E_{T\mathrm{spec}} > 25$ GeV. Also, only ee and $\mu\mu$ events are accepted. No requirements are made on the jet multiplicity or the dilepton invariant mass. The predicted and observed yields for this control region (subsequent to the application of tunings to the Drell-Yan model) are shown in Table XX.

Boson Radiation and heavy flavor resonances are studies using the low $M_{\ell\ell}$ selection described in Section IV B but for $15 < \not\!\!E_{T\mathrm{spec}} < 25$. The predicted and observed yields for this control region are shown in Table XVI.

IX. RESULTS

In order to extract Higgs production limits, we construct a binned likelihood using twelve neural network templates: two templates each for the 0-jet and 1-jet channels (high S/B and low S/B), one template for the 2 or more jets channel, one template for the low $M_{\ell\ell}$ channel, one template for the same-sign channel, one template for each of the three trilepton channels, and two additional templates obtained from an analysis of opposite-sign channels where one lepton is identified as a hadronic tau candidate [48]. All the signals and backgrounds are allowed to float, but ratios of signal and background contributions are constrained to their expectations within a set of Gaussian constraints that are determined from the assumed correlations between the systematics uncertainties. The total signal yield is also allowed to float.

Expected 95% C.L. limits are determined using 10,000 Monte Carlo background-only experiments based on expected yields varied within the assigned systematics. Again, correlations between the systematics for different backgrounds are included. For each experiment a test statistic is formed from the difference in the likelihood value for the background-only model versus that for the signal plus background model.

In the opposite-sign event sample we observe (summing over all jet multiplicities) a total of 4167 candidate events compared against an expectation of 4040 ± 340 background events and 63.0 ± 9.1 signal events for a SM Higgs boson with a mass of 165 GeV/c^2. In the opposite-sign low dilepton invariant mass sample we observe 319 candidate events compared against an expectation of 291 ± 19 background events and 4.41 ± 0.68 signal events for a SM Higgs boson with a mass of 165 GeV/c^2. In the same-sign event sample we additionally observe 87 candidate events compared with an expectation of 85 ± 18 background events and 3.08 ± 0.41 signal events for a SM Higgs boson with a mass of 165 GeV/c^2. In the trilepton event sample we observe 84 candidate events compared with an expectation of 79.2 ± 9.5 background events and 2.49 ± 0.34 signal events for a SM Higgs boson with a mass of 165 GeV/c^2. Table X shows

the expected and observed SM production limits obtained for nineteen different Higgs mass hypotheses in the range from 110 to 200 GeV/c^2. The median, background-only expected 95% C.L. production limit for a Higgs mass of 165 GeV/c^2 is 0.69 times the SM prediction, while the observed limit is 0.40 times the SM prediction. Based on the observed limits we exclude at 95% C.L. a SM Higgs boson with mass between 148 and 175 GeV/c^2.

TABLE X: Expected and observed 95% C.L. Higgs production limits with respect to SM predictions for nineteen different Higgs mass hypotheses using 9.7 fb^{-1} of integrated luminosity.

High Mass	110	115	120	125	130	135	140	145	150	155	160	165	170	175	180	185	190	195	200
$-2\sigma/\sigma_{SM}$	5.39	2.95	1.88	1.29	0.96	0.74	0.64	0.52	0.46	0.40	0.32	0.30	0.34	0.42	0.47	0.58	0.75	0.86	1.00
$-1\sigma/\sigma_{SM}$	8.61	4.71	2.97	2.05	1.52	1.22	1.01	0.86	0.74	0.64	0.48	0.46	0.54	0.65	0.75	0.96	1.18	1.40	1.59
Median/$\sigma_{\mathbf{SM}}$	**13.06**	**7.07**	**4.47**	**3.08**	**2.29**	**1.85**	**1.53**	**1.31**	**1.13**	**0.96**	**0.71**	**0.69**	**0.81**	**0.97**	**1.13**	**1.46**	**1.80**	**2.10**	**2.42**
$+1\sigma/\sigma_{SM}$	19.03	10.25	6.51	4.49	3.34	2.67	2.24	1.91	1.66	1.41	1.03	0.99	1.19	1.41	1.65	2.15	2.63	3.10	3.57
$+2\sigma/\sigma_{SM}$	26.57	14.32	9.21	6.28	4.62	3.75	3.17	2.69	2.32	1.97	1.43	1.39	1.65	1.95	2.31	2.99	3.71	4.30	4.99
Observed/$\sigma_{\mathbf{SM}}$	**17.28**	**11.52**	**4.96**	**2.98**	**2.81**	**1.85**	**1.84**	**1.22**	**0.94**	**0.83**	**0.50**	**0.40**	**0.84**	**0.99**	**1.26**	**1.87**	**2.56**	**5.10**	**5.33**

Considering only the gluon fusion ($gg \to H \to W^+W^-$) production process we obtain 95% C.L. upper limits on the production cross section times branching ratio for this process. These limits (in *pb*) are shown in Table XI for twenty-nine different Higgs mass hypotheses in the range from 110 to 300 GeV/c^2. From these limits we exclude at 95% C.L. a SM-like Higgs boson in the mass range between 124 and 202 GeV/c^2 for the scenario of a fourth sequential generation of fermions with large masses.

TABLE XI: Expected and observed 95% C.L. upper limits on the gluon fusion production cross section times $H \to WW$ branching fraction for twenty-nine different Higgs mass hypotheses using 8.2 fb^{-1} of integrated luminosity.

m_H (GeV/c^2)	obs (pb)	-2σ exp (pb)	-1σ exp (pb)	Median exp (pb)	$+1\sigma$ exp (pb)	$+2\sigma$ exp (pb)
110	0.90	0.77	1.08	1.56	2.25	3.19
115	0.89	0.66	0.90	1.26	1.79	2.50
120	0.94	0.58	0.83	1.18	1.66	2.28
125	0.88	0.53	0.74	1.05	1.49	2.09
130	0.78	0.49	0.69	0.98	1.39	1.92
135	1.02	0.48	0.66	0.94	1.33	1.85
140	0.97	0.43	0.61	0.87	1.24	1.73
145	0.74	0.40	0.55	0.80	1.14	1.60
150	0.64	0.39	0.52	0.73	1.02	1.43
155	0.68	0.32	0.44	0.61	0.86	1.18
160	0.38	0.23	0.31	0.44	0.63	0.89
165	0.40	0.22	0.29	0.41	0.58	0.82
170	0.48	0.27	0.32	0.44	0.64	0.95
175	0.44	0.26	0.35	0.50	0.71	0.99
180	0.49	0.29	0.37	0.52	0.75	1.08
185	0.52	0.29	0.40	0.57	0.81	1.13
190	0.76	0.29	0.41	0.58	0.83	1.16
195	0.77	0.31	0.44	0.62	0.88	1.22
200	0.79	0.32	0.44	0.63	0.89	1.23
210	0.84	0.33	0.45	0.65	0.94	1.32
220	0.80	0.31	0.44	0.63	0.89	1.24
230	0.73	0.30	0.42	0.59	0.84	1.17
240	0.84	0.31	0.43	0.60	0.83	1.13
250	0.55	0.26	0.37	0.52	0.74	1.03
260	0.52	0.24	0.33	0.46	0.65	0.91
270	0.43	0.22	0.29	0.41	0.59	0.85
280	0.49	0.19	0.27	0.37	0.52	0.72
290	0.38	0.19	0.25	0.35	0.50	0.71
300	0.31	0.18	0.23	0.32	0.44	0.62

To determine limits on fermiophobic Higgs production, we remove gluon fusion SM Higgs production and add the $H \to \gamma\gamma$ final state. We extract 95% C.L. upper limits on the production cross section times branching ratio for this process in the range between 100 GeV/c^2 and 150 GeV/c^2. For this scenario we exclude at the 95% C.L. a fermiophobic Higgs boson in the mass range between 100 and 115 GeV/c^2. These limits are shown in Table XII.

Table XIII gives the branching ratios for fermiphobic Higgs production used in this analysis for each mass investigated as calculated using HDECAY [2]. Further details on the $H \to \gamma\gamma$ analysis can be found in [8].

TABLE XII: Expected and observed 95% C.L. upper limits on fermiophobic Higgs production with respect to prediction for eleven different Higgs mass hypotheses using up to 9.7 fb^{-1} of integrated luminosity.

m_H (GeV/c^2)	obs (Limit/FP Model)	-2σ exp (Limit/FP Model)	-1σ exp (Limit/FP Model)	Median exp (Limit/FP Model)	$+1\sigma$exp (Limit/FP Model)	$+2\sigma$exp (Limit/FP Model)
100	0.18	0.12	0.15	0.21	0.30	0.42
105	0.43	0.21	0.29	0.41	0.58	0.80
110	0.60	0.31	0.43	0.59	0.82	1.13
115	1.00	0.44	0.60	0.84	1.18	1.64
120	1.07	0.51	0.72	1.02	1.43	1.96
125	1.15	0.63	0.84	1.15	1.60	2.20
130	1.57	0.69	0.93	1.30	1.82	2.52
135	1.77	0.71	0.97	1.36	1.92	2.69
140	1.82	0.79	1.06	1.47	2.04	2.81
145	1.60	0.82	1.11	1.56	2.21	3.10
150	1.46	0.85	1.13	1.59	2.25	3.16
155	1.61	0.86	1.14	1.59	2.24	3.13
160	1.12	0.85	1.11	1.52	2.12	2.94
165	1.21	0.83	1.10	1.54	2.15	2.99
170	1.65	0.93	1.23	1.70	2.40	3.36
175	1.88	1.05	1.39	1.94	2.74	3.85
180	2.17	1.14	1.57	2.20	3.08	4.24
185	2.83	1.35	1.85	2.61	3.69	5.13
190	4.17	1.69	2.22	3.03	4.19	5.77
195	5.10	1.97	2.59	3.59	5.04	7.03
200	5.48	2.14	2.84	3.95	5.56	7.77

X. SUMMARY

We have searched for SM Higgs boson decay to WW^* in dilepton and trilepton plus $\not\!\!E_T$ final states using a combined Matrix Element and neural network technique. The observed 95% C.L. production limits compare well with background-only expected limits over a wide range of potential Higgs mass values as illustrated in Table X and Fig. 19. We observe no sign of a significant signal excess or deficit over the studied range of Higgs masses. We also specifically search for gluon fusion Higgs production using a 8.2 fb^{-1} data sample and set 95% C.L. upper limits on the production cross section times $H \to WW$ branching fraction as shown in Table XI and Fig. 18(a). As illustrated in Fig. 18(b), these cross section limits are used to constrain the mass of a SM-like Higgs boson in the scenario of a fourth generation of sequential fermions with large masses. We additionally set 95% C.L. production limits on fermiophobic Higgs production as shown in Table XII and Fig. 19.

[1] The LEP Electroweak Working Group, http://lepewwg.web.cern.ch/LEPEWWG/.
[2] A. Djouadi, J. Kalinowski, and M. Spira, Comput. Phys. Commun. **108**, 56 (1998).
[3] D. de Florian and M. Grazzini, Phys. Lett. B **674**, 291 (2009).
[4] C. Anastasiou, R. Boughezal, and F. Petriello, JHEP **0904**, 003 (2009).
[5] M. Feindt and U. Kerzel, Nucl. Instrum. Methods A **559**, 190 (2006).
[6] J. Campbell and K. Ellis, MCFM - Monte Carlo for FeMtobarn processes, http://mcfm.fnal.gov/.
[7] G. D. Kribs, T. Plehn, M. Spannowsky, and T. T. M., Phys. Rev. D **76**, 075016 (2007).
[8] T. Aaltonen *et al.* (CDF Collaboration) (2011), http://www-cdf.fnal.gov/physics/new/hdg/Results_files/results/hgamgam_apr/10485_HiggsGamGam7Public.pdf.
[9] R. Blair, *et al.* (CDF Collaboration) (1996), FERMILAB-PUB-96/390-E.
[10] A. Sill *et al.* (CDF Collaboration), Nucl. Instrum. Methods A **447**, 1 (2000).
[11] A. Affolder *et al.* (CDF Collaboration), Nucl. Instrum. Methods A **453**, 84 (2000).
[12] T. Affolder *et al.* (CDF Collaboration), Nucl. Instrum. Methods A **526**, 249 (2004).
[13] J. A. et al., JHEP **09**, 028 (2007).
[14] R. Brun, R. Hagelberg, M. Hansroul, and J. C. Lassalle, CERN-DD-78-2-REV and CERN-DD-78-2.

TABLE XIII: Decay branching fractions of the Higgs boson in the Fermiophobic Higgs model computed with HDECAY [2].

m_H (GeV)	$\gamma\gamma$	$Z\gamma$	W^+W^-	ZZ	Γ_H (GeV)
100	0.1846	0.3848E-02	0.7353	0.7625E-01	0.3563E-04
105	0.1042	0.6793E-02	0.8157	0.7328E-01	0.7490E-04
110	0.6027E-01	0.8163E-02	0.8527	0.7883E-01	0.1530E-03
115	0.3658E-01	0.8360E-02	0.8664	0.8866E-01	0.2968E-03
120	0.2334E-01	0.7945E-02	0.8694	0.9928E-01	0.5465E-03
125	0.1556E-01	0.7266E-02	0.8684	0.1087	0.9624E-03
130	0.1073E-01	0.6498E-02	0.8667	0.1160	0.1638E-02
135	0.7586E-02	0.5718E-02	0.8662	0.1205	0.2724E-02
140	0.5441E-02	0.4951E-02	0.8682	0.1214	0.4485E-02
145	0.3902E-02	0.4194E-02	0.8741	0.1178	0.7440E-02
150	0.2733E-02	0.3417E-02	0.8861	0.1077	0.1282E-01
155	0.1761E-02	0.2544E-02	0.9086	0.8706E-01	0.2471E-01
160	0.8351E-03	0.1420E-02	0.9512	0.4655E-01	0.7191E-01
165	0.3343E-03	0.6422E-03	0.9754	0.2359E-01	0.2238
170	0.2256E-03	0.4622E-03	0.9748	0.2456E-01	0.3519
175	0.1791E-03	0.3877E-03	0.9663	0.3315E-01	0.4675
180	0.1484E-03	0.3367E-03	0.9386	0.6093E-01	0.5927
185	0.1178E-03	0.2787E-03	0.8479	0.1517	0.7804
190	0.9789E-04	0.2402E-03	0.7881	0.2116	0.9782
195	0.8522E-04	0.2160E-03	0.7590	0.2407	1.167
200	0.7589E-04	0.1980E-03	0.7423	0.2575	1.356
205	0.6848E-04	0.1834E-03	0.7316	0.2681	1.553
210	0.6234E-04	0.1709E-03	0.7243	0.2755	1.758
215	0.5709E-04	0.1599E-03	0.7190	0.2807	1.974
220	0.5251E-04	0.1500E-03	0.7151	0.2847	2.203
225	0.4849E-04	0.1410E-03	0.7120	0.2878	2.446
230	0.4490E-04	0.1328E-03	0.7094	0.2904	2.703
235	0.4170E-04	0.1251E-03	0.7073	0.2925	2.976
240	0.3881E-04	0.1181E-03	0.7055	0.2943	3.265
245	0.3620E-04	0.1116E-03	0.7039	0.2959	3.570
250	0.3382E-04	0.1055E-03	0.7024	0.2974	3.892
255	0.3166E-04	0.9983E-04	0.7011	0.2988	4.233
260	0.2968E-04	0.9455E-04	0.6999	0.3000	4.592

[15] S. Frixione and B. R. Webber, JHEP **0206**, 029 (2002).
[16] T. Sjostrand, L. Lonnblad, and S. Mrenna (2001), hep-ph/0108264.
[17] U. Baur and E. L. Berger, Phys. Rev. D **47**, 4889 (1993).
[18] H. L. Lai *et al.* (CTEQ Collaboration), Phys. Rev. D **55**, 1280 (1997).
[19] R. Harlander and W. B. Kilgore, Phys. Rev. Lett. **88**, 201801 (2002).
[20] C. Anastasiou and K. Melnikov, Nucl. Phys. B **646**, 220 (2002).
[21] V. Ravindran, J. Smith, and W. L. van Neerven, Nucl. Phys. B **665**, 325 (2003).
[22] S. Actis, G. Passarino, C. Sturm, and S. Uccirati, Phys. Lett. B **670**, 12 (2008).
[23] U. Aglietti, R. Bonciani, G. Degrassi, and A. Vicini (2006), hep-ph/0610033v1.
[24] S. Catani, D. de Florian, M. Grazzini, and P. Nason, JHEP **0307**, 028 (2003).
[25] K. A. Assamagan *et. al.* (Higgs working group) (2004), hep-ph/0406152.
[26] O. Brein, A. Djouadi, and R. Harlander, Phys. Lett. B **579**, 149 (2004).
[27] M. L. Ciccolini, S. Dittmaier, and M. Kramer, Phys. Rev. D **68**, 073003 (2003).
[28] J. Baglio and A. Djouadi (2010), arXiv:1003.4266v2 [hep-ph].
[29] E. Berger and J. Campbell, Phys. Rev. D **70**, 073011 (2004).
[30] F. Bolzoni, F. Maltoni, M. S.-O., and M. Zaro (2010), arXiv:1003.4451 [hep-ph].
[31] A. D. Martin, W. J. Stirling, R. S. Thorne, and G. Watt, Eur. Phys. J. C **63**, 189 (2009).
[32] J. M. Campbell and R. K. Ellis, Phys. Rev. D **60**, 113006 (1999).
[33] U. Langenfeld, S. Moch, and P. Uwer, Phys. Rev. D **80**, 054009 (2009).
[34] N. Kidonakis and R. Vogt, Phys. Rev. D **78**, 074005 (2008).
[35] M. Cacciari, S. Frixione, M. L. Mangano, P. Nason, and G. Ridolfi, JHEP **0809**, 127 (2008).
[36] D. Acosta *et al.* (CDF Collaboration), Nucl. Instrum. Methods A **494**, 57 (2002).
[37] The TeV4LHC Working Group, http://maltoni.home.cern.ch/maltoni/TeV4LHC/SM.html.
[38] M. Grazzini, HNNLO, http://theory.fi.infn.it/grazzini/codes.html.
[39] S. Catani and M. Grazzini, Phys. Rev. Lett. **98**, 222002 (2007).

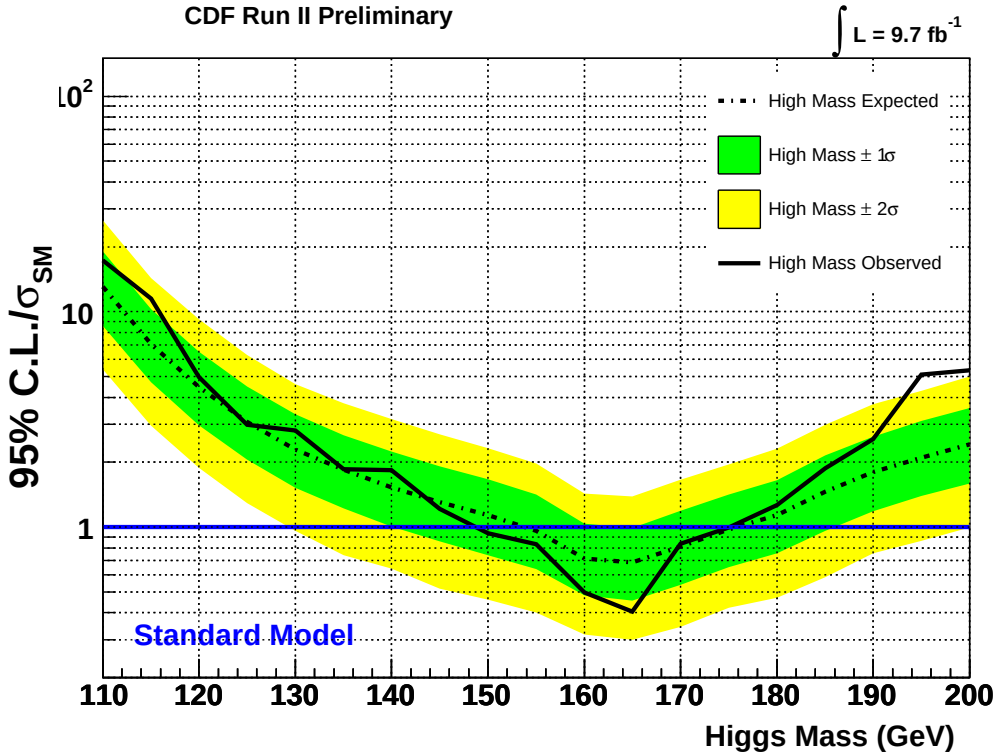

FIG. 17: The observed (solid black line) and median expected (dashed black line) 95% C.L. upper limits on Higgs production relative to the SM prediction. The shaded bands around the median prediction indicate the ±1 and ±2 standard deviations expected for a single experiment if a Higgs boson signal is not present. The current LEP mass exclusion range and the mass range excluded from this search are indicated by the vertical shaded bands.

[40] M. Grazzini, JHEP **0802**, 043 (2008).
[41] C. Anastasiou, G. Dissertori, M. Grazzini, F. Stoeckli, and B. R. Webber, JHEP **0908**, 099 (2009).
[42] J. Campbell, R. Ellis, and C. Williams, Phys. Rev. D **81**, 074023 (2010).
[43] G. Bozzi, S. Catani, D. deFlorian, and M. Grazzini, Phys. Lett. B **564**, 65 (2003).
[44] G. Bozzi, S. Catani, D. deFlorian, and M. Grazzini, Nucl. Phys. B **737**, 73 (2006).
[45] C. Balazs, J. Huston, and I. Puljak, Phys. Rev. D **63**, 014021 (2001).
[46] C. Balazs and C.-P. Yuan, Phys. Lett. B **478**, 192 (2000).
[47] Q.-H. Cao and C.-R. Chen, Phys. Rev. D **76**, 073006 (2007).
[48] M. Bauce, *et al.* (CDF Collaboration) (2012), http://www-cdf.fnal.gov/cdfnotes/cdf10781_HWW_tau_97fb_public.pdf.

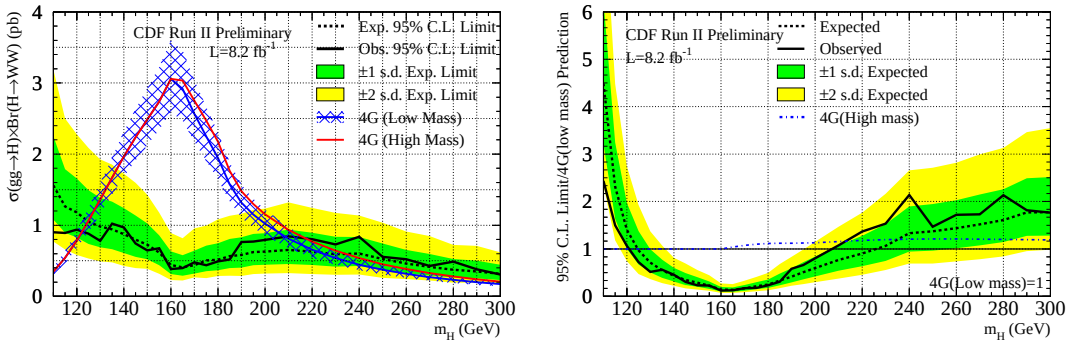

FIG. 18: The observed (solid black lines) and median expected (dashed black lines) 95% C.L. upper limits on $\sigma(gg \to H) \times B(H \to W^+W^-)$ are shown in figure (a). The shaded bands indicate the ± 1 standard deviation (s.d.) and ± 2 s.d. intervals on the distribution of the limits that are expected if a Higgs boson signal is not present. Also shown on each graph is the prediction for a fourth-generation model in the low-mass and high-mass scenarios, 4G (Lowmass) and 4G (Highmass) respectively. The hatched areas indicate the theoretical uncertainty from PDF and scale uncertainties. The lighter curves show the high-mass theoretical prediction. Figure (b) shows the 95% C.L. limit relative to the low-mass theoretical prediction, where the uncertainties in the signal prediction are included in the limit. Also shown in Figure (b) is the prediction of the signal rate in the high-mass scenario, divided by that of the low-mass scenario.

TABLE XIV: Expected and observed yields in the $W\gamma$ control sample based on Monte Carlo predictions using the Bauer Monte Carlo and after rescaling the $W\gamma$ Monte Carlo to data.

Category	WW	WZ	ZZ	$t\bar{t}$	DY	$W\gamma$	W+jets	Total	Data
e e	0.14	0.17	0.01	0.01	0.53	77.65	9.28	87.78	107
e μ	0.08	0.37	0.03	0	6.27	42.24	5.4	54.39	51
μ μ	0	0.2	0.02	0	0	0	0.91	1.14	1
e trk	0.04	0.06	0	0	1.18	12.53	19.18	32.99	24
μ trk	0	0.05	0	0	0.15	3.29	8.25	11.74	5
Total:	0.26	0.86	0.06	0.02	8.12	135.71	43.02	188.04	188

TABLE XV: Expected and observed yields in the $W\gamma$ control sample based on Monte Carlo Predictions using MadGraph4 [13].

Category	WW	WZ	ZZ	$t\bar{t}$	DY	$W\gamma$	W+jets	Total	Data
e e	0.14	0.18	0.01	0.01	0.53	97.1	9.62	107.58	128
e μ	0.08	0.4	0.03	0	6.82	60.38	6.74	74.44	71
μ μ	0	0.23	0.02	0	0	0	1	1.25	4
e trk	0.04	0.06	0	0	1.18	12.99	19.18	33.46	24
μ trk	0	0.05	0	0	0.15	2.67	9.31	12.18	5
Total:	0.26	0.92	0.06	0.02	8.67	173.13	45.85	228.91	232

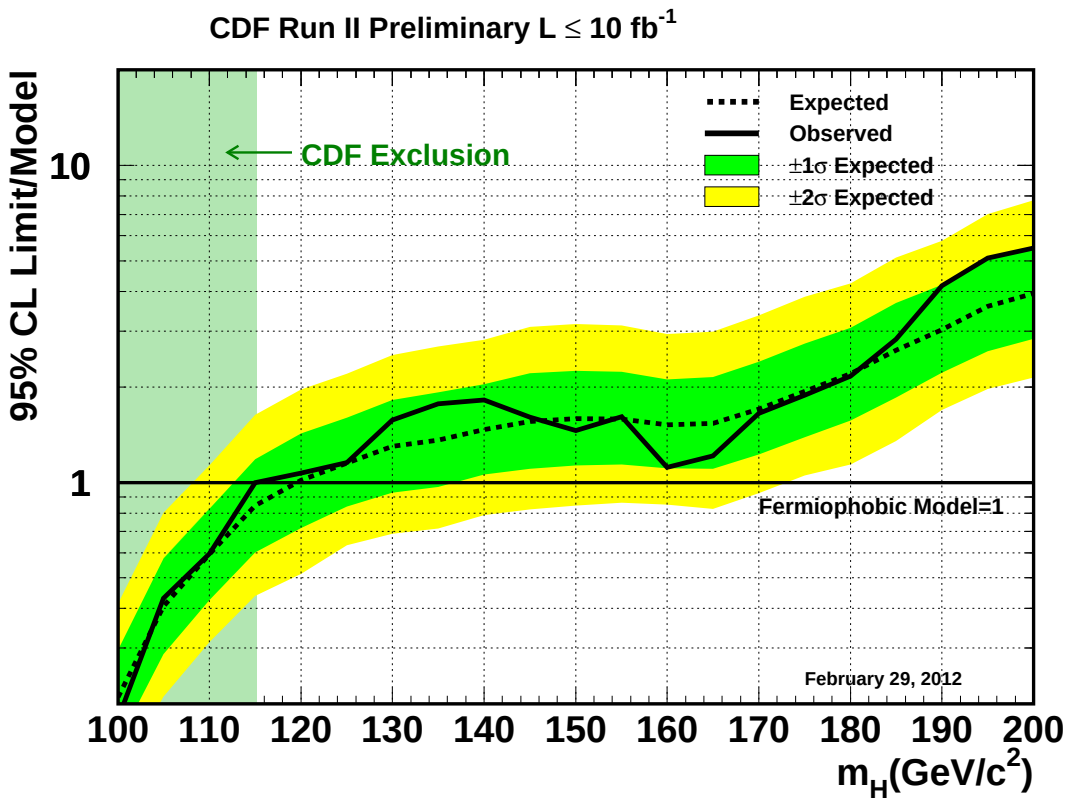

FIG. 19: The observed (solid black line) and median expected (dashed black line) 95% C.L. upper limits on fermiophobic Higgs production relative to prediction. The shaded bands around the median prediction indicate the ±1 and ±2 standard deviations expected for a single experiment if a Higgs boson signal is not present. The current LEP mass exclusion range and the mass range excluded from this search are indicated by the vertical shaded bands.

TABLE XVI: Expected and observed yields in the Low $\not\!\!E'_{T\,\mathrm{spec}}$ control sample based on Monte Carlo Predictions using MadGraph4 [13].

Category	WW	WZ	ZZ	$t\bar{t}$	DY	$W\gamma$	W+jets	Total	Data
$e\ e$	0.14	0.02	0.01	0.03	37.85	1.97	2.32	42.34	44
$e\ \mu$	0.14	0.01	0	0.03	0.15	0.5	0.5	1.34	0
$\mu\ \mu$	0.17	0.01	0.01	0.03	24.73	0	0.19	25.14	26
e trk	0.06	0.01	0	0.01	4.48	0.37	2.17	7.09	14
μ trk	0.04	0	0	0	3.05	0.06	3.24	6.4	2
Total:	0.56	0.06	0.02	0.11	70.26	2.9	8.41	82.31	86

TABLE XVII: Expected and observed yields in the $t\bar{t}$ control sample.

Category	WW	WZ	ZZ	$t\bar{t}$	DY	$W\gamma$	W+jets	Total	Data
$e\ e$	0.1	0.1	0.1	66.5	0.0	0.1	1.4	68.2	52.0
$e\ \mu$	0.2	0.1	0.1	144.4	1.3	0.0	1.8	147.7	137.0
$\mu\ \mu$	0.1	0.1	0.0	45.2	0.2	0.0	1.1	46.6	53.0
e trk	0.1	0.0	0.1	43.2	0.0	0.0	2.1	45.5	35.0
μ trk	0.0	0.0	0.0	26.4	0.0	0.0	3.9	30.4	30.0
Total:	0.5	0.3	0.3	325.6	1.5	0.1	10.2	338.4	307.0

TABLE XVIII: Expected and observed yields in the W+jets control sample.

Category	WW	WZ	ZZ	$t\bar{t}$	DY	$W\gamma$	W+jets	Total	Data
$e\ e$	0.0	0.6	0.0	0.0	24.4	3.0	10.4	38.3	52.0
$e\ \mu$	0.0	4.1	0.2	0.0	6.6	5.2	27.4	43.5	30.0
$\mu\ \mu$	0.0	4.0	0.4	0.0	2.9	0.0	12.8	20.1	34.0
e trk	0.0	1.2	0.1	0.0	20.5	3.2	111.3	136.2	116.0
μ trk	0.0	2.9	0.2	0.0	4.0	1.6	31.8	40.4	22.0
Total:	0.1	12.7	0.8	0.0	58.4	12.9	193.6	278.6	254.0

TABLE XIX: Expected and observed yields in the inclusive Drell-Yan control sample.

Category	WW	WZ	ZZ	$t\bar{t}$	DY	$W\gamma$	W+jets	Total	Data
$e\ e$	21.0	135.5	122.0	5.6	371364.8	5.1	1154.1	372808.2	345852.0
$e\ \mu$	18.4	0.4	0.2	4.0	334.1	1.5	75.2	433.9	356.0
$\mu\ \mu$	17.2	91.5	85.8	4.3	245931.8	0.0	1043.9	247174.5	242994.0
e trk	15.9	39.7	36.8	4.1	106188.1	1.0	5142.2	111427.8	99665.0
μ trk	9.7	26.0	23.9	2.5	70191.5	0.1	4186.3	74440.0	66644.0
Total:	82.2	293.1	268.7	20.5	794010.3	7.8	11601.6	806284.2	755511.0

TABLE XX: Expected and observed yields in the intermediate $\not\!\!E_T$ Drell-Yan control sample.

Category	WW	WZ	ZZ	$t\bar{t}$	DY	$W\gamma$	W+jets	Total	Data
$e\ e$	12.1	9.4	9.3	6.9	5715.2	3.7	44.3	5800.8	5813.0
$e\ \mu$	0.0	0.0	0.0	0.0	0.0	0.0	0.0	0.0	0.0
$\mu\ \mu$	9.2	5.8	6.1	5.1	2685.7	0.0	21.2	2733.1	2844.0
e trk	9.2	3.2	3.1	5.1	1812.5	0.7	132.4	1966.3	1675.0
μ trk	5.3	1.7	1.7	3.0	740.6	0.1	77.5	829.8	751.0
Total:	35.9	20.0	20.2	20.0	10954.0	4.5	275.3	11330.0	11083.0

TABLE XXI: Systematics for opposite-sign lepton with zero jet channels.

Uncertainty Source	WW	WZ	ZZ	$t\bar{t}$	DY	$W\gamma$	W+jet	$gg \to H$	WH	ZH	VBF
Cross Section											
ScaleInclusive								13.4%			
Scale1+Jets								−23.0%			
Scale2+Jets								0.0%			
PDF Model								7.6%			
Total	*6.0%*	*6.0%*	*6.0%*	7.0%					**5.0%**	**5.0%**	10.0%
Acceptance											
Scale (jets)	*0.3%*s										
PDF Model (leptons)								2.7%			
PDF Model (jets)	*1.1%*							5.5%			
Higher-order Diagrams		*10.0%*	*10.0%*	10.0%		10.0%			**10.0%**	**10.0%**	**10.0%**
$\not\!\!E_T$ Modeling					19.0%						
Conversion Modeling						6.8%					
Jet Fake Rates											
(Low S/B)							15.0%				
(High S/B)							24.0%				
Jet Energy Scale	*3.1%*	*6.2%*	*3.5%*	*28.2%*	*18.0%*	*3.5%*		*5.7%*	*9.9%*	*5.3%*	*12.9%*
Lepton ID Efficiencies	*3.8%*	*3.8%*	*3.8%*	*3.8%*	*3.8%*			*3.8%*	*3.8%*	*3.8%*	*3.8%*
Trigger Efficiencies	*2.0%*	*2.0%*	*2.0%*	*2.0%*	*2.0%*			*2.0%*	*2.0%*	*2.0%*	*2.0%*
Luminosity	*5.9%*	*5.9%*	*5.9%*	*5.9%*	*5.9%*			*5.9%*	*5.9%*	*5.9%*	*5.9%*

TABLE XXII: Systematics for opposite-sign lepton with one jet channels.

Uncertainty Source	WW	WZ	ZZ	$t\bar{t}$	DY	$W\gamma$	W+jet	$gg \to H$	WH	ZH	VBF
Cross Section											
ScaleInclusive								0.0%			
Scale1+Jets								35.0%			
Scale2+Jets								−12.7%			
PDF Model								17.3%			
Total	*6.0%*	*6.0%*	*6.0%*	7.0%					**5.0%**	**5.0%**	10.0%
Acceptance											
Scale (jets)	*-4.0%*s										
PDF Model (leptons)								3.6%			
PDF Model (jets)	*4.7%*							-6.3%			
Higher-order Diagrams		*10.0%*	*10.0%*	10.0%		10.0%			**10.0%**	**10.0%**	**10.0%**
$\not{E}_T$ Modeling					21.0%						
Conversion Modeling						6.8%					
Jet Fake Rates											
(Low S/B)							16.0%				
(High S/B)							27.0%				
Jet Energy Scale	*-5.8%*	*-1.1%*	*-4.8%*	*-13.1%*	*-6.5%*	*-9.5%*		*-3.8%*	*-8.5%*	*-7.8%*	*-6.8%*
Lepton ID Efficiencies	*3.8%*	*3.8%*	*3.8%*	*3.8%*	*3.8%*			*3.8%*	*3.8%*	*3.8%*	*3.8%*
Trigger Efficiencies	*2.0%*	*2.0%*	*2.0%*	*2.0%*	*2.0%*			*2.0%*	*2.0%*	*2.0%*	*2.0%*
Luminosity	*5.9%*	*5.9%*	*5.9%*	*5.9%*	*5.9%*			*5.9%*	*5.9%*	*5.9%*	*5.9%*

TABLE XXIII: Systematics for opposite-sign lepton with two or more jet channel.

Uncertainty Source	WW	WZ	ZZ	$t\bar{t}$	DY	$W\gamma$	W+jet	$gg \to H$	WH	ZH	VBF
Cross Section											
ScaleInclusive								0.0%			
Scale1+Jets								0.0%			
Scale2+Jets								33.0%			
PDF Model								29.7%			
Total	*6.0%*	*6.0%*	*6.0%*	7.0%					**5.0%**	**5.0%**	10.0%
Acceptance											
Scale (jets)	*-8.2%*s										
PDF Model (leptons)								4.8%			
PDF Model (jets)	*4.2%*							-12.3%			
Higher-order Diagrams		*10.0%*	*10.0%*	10.0%		10.0%			**10.0%**	**10.0%**	**10.0%**
$\not{E}_T$ Modeling					26.0%						
Conversion Modeling						6.8%					
Jet Fake Rates							19.0%				
Jet Energy Scale	*-20.5%*	*-13.2%*	*-13.3%*	*-1.7%*	*-32.7%*	*-22.0%*		*-15.1%*	*-4.0%*	*-2.5%*	*-3.8%*
b-tag Veto				3.6%							
Lepton ID Efficiencies	*3.8%*	*3.8%*	*3.8%*	*3.8%*	*3.8%*			*3.8%*	*3.8%*	*3.8%*	*3.8%*
Trigger Efficiencies	*2.0%*	*2.0%*	*2.0%*	*2.0%*	*2.0%*			*2.0%*	*2.0%*	*2.0%*	*2.0%*
Luminosity	*5.9%*	*5.9%*	*5.9%*	*5.9%*	*5.9%*			*5.9%*	*5.9%*	*5.9%*	*5.9%*

TABLE XXIV: Systematics for opposite-sign lepton, low $M_{\ell\ell}$ with zero or one jet channel.

Uncertainty Source	WW	WZ	ZZ	$t\bar{t}$	DY	$W\gamma$	W+jet(s)	$gg \to H$	WH	ZH	VBF
Cross Section											
ScaleInclusive								8.1%			
Scale1+Jets								0.0%			
Scale2+Jets								−5.1%			
PDF Model								10.5%			
Total	*6.0%*	*6.0%*	*6.0%*	7.0%	5.0%				**5.0%**	**5.0%**	10.0%
Acceptance											
Scale (jets)	*-0.4%*s										
PDF Model (leptons)								1.0%			
PDF Model (jets)	*1.6%*							2.1%			
Higher-order Diagrams		*10.0%*	*10.0%*	10.0%	10.0%				**10.0%**	**10.0%**	**10.0%**
Conversion Modeling						8.4%					
Jet Fake Rates							13.8%				
Jet Energy Scale	*1.2%*	*2.2%*	*2.0%*	*13.3%*	*15.4%*	*1.2%*		*2.4%*	*9.2%*	*6.5%*	*7.8%*
Lepton ID Efficiencies	*3.8%*	*3.8%*	*3.8%*	*3.8%*	*3.8%*			*3.8%*	*3.8%*	*3.8%*	*3.8%*
Trigger Efficiencies	*2.0%*	*2.0%*	*2.0%*	*2.0%*	*2.0%*			*2.0%*	*2.0%*	*2.0%*	*2.0%*
Luminosity	*5.9%*	*5.9%*	*5.9%*	*5.9%*	*5.9%*			*5.9%*	*5.9%*	*5.9%*	*5.9%*

TABLE XXV: Systematics for same-sign lepton with one or more jets channel.

Uncertainty Source	WW	WZ	ZZ	$t\bar{t}$	DY	$W\gamma$	W+jet	WH	ZH
Cross Section									
Total	*6.0%*	*6.0%*	*6.0%*	7.0%	5.0%			**5.0%**	**5.0%**
Acceptance									
Scale (jets)	-6.1%								
PDF Model (jets)	5.7%								
Higher-order Diagrams		*10.0%*	*10.0%*	10.0%	10.0%	10.0%		**10.0%**	**10.0%**
Conversion Modeling						6.8%			
Jet Fake Rates							37.7%		
Charge Mismeasurement Rate	*25.0%*				*25.0%*				
Jet Energy Scale	*-4.1%*	*-4.2%*s	*-3.3%*s	*-0.3%*	*-4.9%*s	*-9.1%*		*-1.0%*s	*-0.7%*s
Lepton ID Efficiencies	*3.8%*	*3.8%*	*3.8%*	*3.8%*	*3.8%*			*3.8%*	*3.8%*
Trigger Efficiencies	*2.0%*	*2.0%*	*2.0%*	*2.0%*	*2.0%*			*2.0%*	*2.0%*
Luminosity	*5.9%*	*5.9%*	*5.9%*	*5.9%*	*5.9%*			*5.9%*	*5.9%*

TABLE XXVI: Systematics for the trilepton with one reconstructed jet and a same-flavor opposite-sign dilepton pair in the Z-mass peak channel.

Uncertainty Source	WZ	ZZ	$Z\gamma$	$t\bar{t}$	Z+jet	WH	ZH
Cross Section							
Total	*6.0%*	*6.0%*	10.0%	7.0%		**5.0%**	**5.0%**
Acceptance							
Higher-order Diagrams	*10.0%*	*10.0%*	15.0%	10.0%		**10.0%**	**10.0%**
Jet Fake Rates					23.6%		
b-Jet Fake Rates				42.0%			
Jet Energy Scale	*-7.8%*	*-2.4%*	*-6.4%*	*2.2%*		*-7.0%*	*7.1%*
Lepton ID Efficiencies	*5.0%*	*5.0%*	*5.0%*	*5.0%*		*5.0%*	*5.0%*
Trigger Efficiencies	*2.0%*	*2.0%*	*2.0%*	*2.0%*		*2.0%*	*2.0%*
Luminosity	*5.9%*	*5.9%*	*5.9%*	*5.9%*		*5.9%*	*5.9%*

TABLE XXVII: Systematics for the trilepton with two or more reconstructed jets and a same-flavor opposite-sign dilepton pair in the Z-mass peak channel.

Uncertainty Source	WZ	ZZ	$Z\gamma$	$t\bar{t}$	Z+jet	WH	ZH
Cross Section							
Total	*6.0%*	*6.0%*	10.0%	7.0%		**5.0%**	**5.0%**
Acceptance							
Higher-order Diagrams	*10.0%*	*10.0%*	15.0%	10.0%		**10.0%**	**10.0%**
Jet Fake Rates					18.4%		
b-Jet Fake Rates				22.2%			
Jet Energy Scale	*-18.0%*	*-15.4%*	*-16.8%*	*-2.3%*		*-20.1%*	*-5.5%*
Lepton ID Efficiencies	*5.0%*	*5.0%*	*5.0%*	*5.0%*		*5.0%*	*5.0%*
Trigger Efficiencies	*2.0%*	*2.0%*	*2.0%*	*2.0%*		*2.0%*	*2.0%*
Luminosity	*5.9%*	*5.9%*	*5.9%*	*5.9%*		*5.9%*	*5.9%*

TABLE XXVIII: Systematics for the trilepton with no same-flavor opposite-sign dilepton pair in the Z-mass peak channel.

Uncertainty Source	WZ	ZZ	$Z\gamma$	$t\bar{t}$	Z+jet	WH	ZH
Cross Section							
Total	*6.0%*	*6.0%*	10.0%	7.0%		**5.0%**	**5.0%**
Acceptance							
Higher-order Diagrams	*10.0%*	*10.0%*	15.0%	10.0%		**10.0%**	**10.0%**
Jet Fake Rates					22.3%		
b-Jet Fake Rates				27.3%			
Jet Energy Scale			*-3.0%*				
Lepton ID Efficiencies	*5.0%*	*5.0%*	*5.0%*	*5.0%*		*5.0%*	*5.0%*
Trigger Efficiencies	*2.0%*	*2.0%*	*2.0%*	*2.0%*		*2.0%*	*2.0%*
Luminosity	*5.9%*	*5.9%*	*5.9%*	*5.9%*		*5.9%*	*5.9%*